Review

Mineral Characterization using Scanning Electron Microscopy (SEM): A Review of the Fundamentals, Advancements, and Research Directions

Asif Ali , Ning Zhang , Rafael M. Santos *

Posted Date: 31 October 2023

doi: 10.20944/preprints202310.2059.v1

Keywords: Scanning electron microscopy; Minerals; Artificial Intelligence; Machine Learning; Energy-dispersive spectrometer; Backscattered electron imaging; Secondary electron imaging

Review

Mineral Characterization using Scanning Electron Microscopy (SEM): A Review of the Fundamentals, Advancements, and Research Directions

Asif Ali [1], Ning Zhang [2] and Rafael M. Santos [1,*]

[1] School of Engineering, University of Guelph, Guelph, ON N1G 2W1, Canada; aali38@uoguelph.ca (AA)
[2] Department of Earth and Environmental Engineering, Columbia University, New York, New York 10027, United States; nz2356@columbia.edu (NZ)
* Correspondence: santosr@uoguelph.ca; Tel.: 1-519-824-4120

Featured Application: The focus of this review is on the use of SEM imaging to gain insights into the composition and morphology of minerals in view of predicting or understanding their reactivity or the process by which they formed.

Abstract: Scanning electron microscopy (SEM) is a powerful tool in the domain of material science, mining, and geology, owing to its enormous potential to provide unique insights into the micro and nanoscale worlds. This comprehensive review discusses the background development of SEM, basic SEM operation including the specimen preparation and imaging process, and fundamental theoretical calculations underlying the SEM operation. It provides foundational understanding to the engineers and scientists, who never got a chance to dig in-depth into the SEM, to understand the working and development of this robust analytical technique. The present review covers how SEM has been serving as a crucial tool in mineral characterization, with specific discussions on the working and research fronts of SEM-EDX, SEM-AM, SEM-MLA, and QEMSCAN. With automation gaining pace in the development of all spheres of technology, the understanding of uncertainties in SEM measurements is very important. The constraints in mineral phase identification by EDS spectra and sample preparation are conferred. In the end, future research directions for SEM are analyzed with the possible incorporation of machine learning, deep learning, and artificial intelligence tools, for automating the process of mineral identification, quantification, and efficient communication with the researchers, so that the analytical process robustness and objectivity can be improved, and the analysis time and the involved costs can be brought down. This review also discusses the idea of integrating robotics with SEM, to make the equipment portable, so that further mineral characterization insights can be gained not only on earth but also on other terrestrial grounds.

Keywords: scanning electron microscopy; minerals; artificial intelligence; machine learning; energy-dispersive spectrometer; backscattered electron imaging; secondary electron imaging

1. Introduction

The rapid pace of technological development requires a detailed study of minerals to a further extent, to meet the unprecedented material demands of the evolving world. There are more than 5956 species of minerals known today and the number of new identifications is evolving with as many as 50 new types identified each year [1,2]. The quantitative measurements and qualitative analyses of mineral compositions within mining ores and reservoirs contain valuable importance to practical applications. A piece of comprehensive and accurate information can be gathered for the identification of rocks and minerals, including structural characteristics and mineral composition, which can provide a worthy set of information about pore structure and reservoir heterogeneity [3–5].

The qualitative analysis of minerals is usually conducted through conventional optical microscopy (OM), also known as light microscopy (LM), scanning electron microscopy (SEM), and infrared spectroscopy methods [6–8]. Mineral characteristics and mutual relationships are broadly

 doi:10.20944/preprints202310.2059.v1

analyzed by OM, however, due to its resolution limitations, it lacks the qualitative analysis of micro-nanoscale particles including structural characteristics and mineral morphology [9,10]. OM can obtain a maximum useful magnification of 1000 times [11]. The wavelength of the imaging radiation can be decreased further for better resolution (i.e., higher useful magnification). OM uses light as imaging radiation, while electron microscopy makes use of electrons to magnify the specimen. Electron beams are accelerated with high energies (from 2 keV to 1000 keV, representing smaller wavelengths of 0.027 nm to 0.0009 nm) in electron microscopes [11].

The bombardment of high-energy electron beams on the atoms in the specimen can result in various possible interactions (**Error! Reference source not found.**), which are subject to the thickness of the specimen. The electrons can be transmitted unabsorbed through the specimen, if its thickness is very small, and can be used to form an image in transmission electron microscopy (TEM) [12]. Contrarily, with thicker specimens, electrons are not transmitted and the particles (electrons, photons, x-rays, etc.) emerging from the surface of the specimen provide morphological and structural information. Low-energy electron beams ranging from 0.1 keV to 30 keV penetrate the sample from a few to tens of nanometers. Medium-energy ones ranging from 30 keV to 1,000 keV penetrate from tens of nanometers to micrometer scale, while high-energy beams, which are usually above 10,000 keV can go from several micrometers to millimeters within the sample. The retrieved information signals are used in SEM to provide sample characteristic information [13].

SEM can be used to analyze the crystalline structure, surface topography, electrical behavior, and chemical composition of around 1μm of the top part of the specimen [11]. The behavior of the specimen under several conditions can be investigated using SEM, as a variety of specialized stages can be attached to it, such as, cold [14], hot [15], or designed to allow in situ mechanical testing [16]. For instance, cathodoluminescence (emission of light) works very well for temperatures near absolute zero, as compared to room temperature [17,18]. Since the images formed are much less noisy from the light emitted by a cold specimen.

SEM has additional advantages over OM. For example, SEM has a powerful useful magnification of 1,000,000 times and can reach up to the nanometer scale [19]. This allows an in-depth examination of the specimen as compared to the OM. Surface smoothness affects the quality of micrographs taken with OM, as high-magnification OM possesses a very low depth of field. SEM, on the other hand, has a large depth of field and it benefits in simultaneous focus on the specimen surface, irrespective of the surface roughness [20]. SEM contains the possibility to go beyond analyzing the surface topography [21], such as chemical composition [22], crystal structure [23], and electrical properties [24]. The confidence of analysis can be gained further by switching between different imaging techniques, which enables cross-correlating the acquired information. SEM is also beneficial over TEM in several analytical scenarios. SEM can cater to larger-sized samples (wafers of 200 mm diameter, while specially adapted SEMs can go further up), in comparison to TEM, which can go to just 2.3 mm or 3 mm [19]. SEM is a non-destructive analytical technique [25], while the specimen preparation process of TEM makes it a destructive technique [26]. The time required for preparing the sample for SEM is also less when compared to the TEM technique.

 doi:10.20944/preprints202310.2059.v1

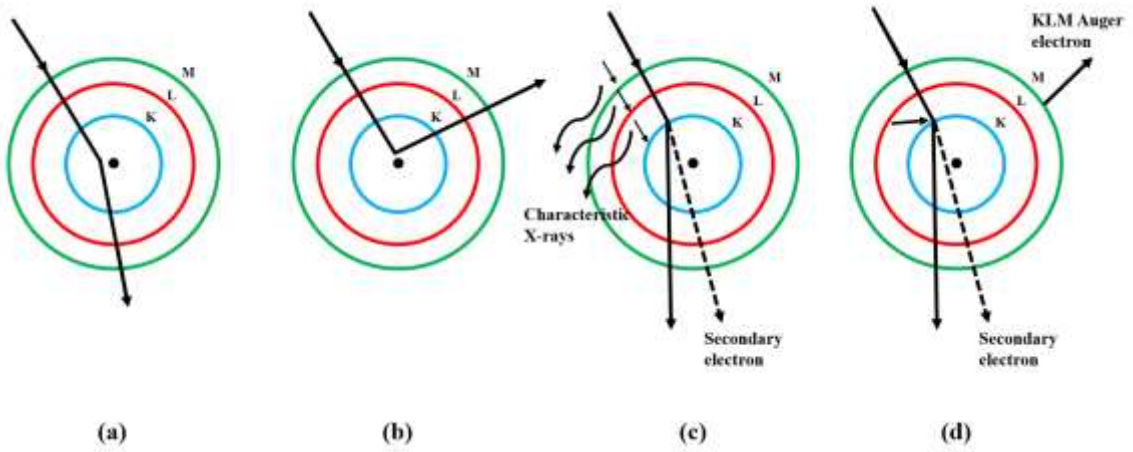

Figure 1. Various possible interactions of high-energy electrons with atoms. The atomic shells are labeled with standard notation (i.e., K, L, M). The incident particle is shown with a solid arrow. (a) Low-angle scattering: very little energy loss is experienced by the incident electrons, and they scatter to the next layer of atoms; (b) High-angle (or back) scattering; (c) Emission of characteristic x-rays and a secondary electron; (d) Emission of an Auger electron and a secondary electron.

SEM can be further classified into three types, i.e., conventional SEM (CSEM), low vacuum SEM (LVSEM), and environmental SEM (ESEM) [27–29]. CSEM usually possesses a high-vacuum (10^{-6} torr) condition for the interaction of electron beam and specimen. This allows the emission of low-energy secondary electrons from the specimen, resulting in their minimum collisions with the gas molecules present in the chamber. The CSEM reinforces those analyses where dehydration and cracking of the sample (due to high vacuum) is not a problem such as the identification of alkali-silica reactivity in concrete [30]. The second type LVSEM is similar to CSEM, with adaptation of elevated pressure (0.2 to 1 torr) operations as well. The LVSEM environment slowly dissipates any liquid water present in the sample, and therefore the crack propagation in the sample moves very slowly. For non-conductive samples, it is important to add the conductive coating to avoid any charging effects. The third type ESEM permits imaging of the sample at high humidity and therefore, is considered as "wet mode". ESEM has a relatively high-pressure environment i.e., 0.2 to 20 torr, which reduces or eliminates dehydration. The elevated pressure reinforces the ionization of gas molecules due to the emission of surface charges, thereby reducing the need for conductive coatings [31]. The strength of the electron signal increases with the ionization of gas molecules, providing better results. ESEM supports coherent imaging but ponders a limited ability for analyzing X-ray microanalysis, as frequent collisions lead to defocusing and scattering of the electron beam which makes the position of the beam on the specimen uncertain. Field emission gun SEM (FEG SEM) typically falls under the category of CSEM, as its operation includes high vacuum conditions. In conclusion, the type of SEM should be chosen based on the nature of the specimen and the required analysis.

1.1. Background Development of SEM

The idea of using electron microscopy dates back to the previous century when Ruska and Knoll conducted their experiments in 1932 [32,33]. This instrument was named as transmission electron microscope (TEM), based on its working principle and application, where electrons were transmitted through thin specimens to magnify beyond levels of the optical microscope of that time. In 1938, a scanning coil was added to the TEM by Von Ardenne, introducing the era of scanning transmission electron microscopy (STEM) [34,35]. It provided a magnification of 8000x with a resolution of 50-100 nm at 23 keV. Ardene developed the laboratory instrument with various features, which became standard for developing and inventing new SEM systems [36]. A new explanation of SEM for analyzing thick samples was presented by Zworykin, Hillier, and Snyder in 1942. It was found that

 doi:10.20944/preprints202310.2059.v1

the emission of secondary electrons can be used for topographic contrast. Oatley and McMullan in 1952 developed the electrostatic lens for SEM. Smith understood the role of signal processing in improving SEM micrographs and laid the foundation for non-linear signal amplification. Another contribution from Smith was the production of double deflection scanning for upgrading the scanning system [36]. Wells in 1953 designed a new stereoscopic pair for investigating the third dimension in SEM micrographs. The work of Everhart and Thornley indicates the development of a secondary detector, which served as a tool for improving the signal-to-noise ratio, and overall increasing the collected signals. Pease used the three magnetic lenses in building the SEM V system, which is considered the first commercial SEM instrument available under the name of "Stereoscan" Cambridge Scientific Instruments Mark 1 in markets from 1965 [37]. Since then, several advancements have been made to improve the SEM analysis, such as the upgradation of electron source for better electron emission resulting in efficient and clear SEM resolution. Another beneficial advancement in SEM development pertains to the invention of an energy-dispersive spectrometer (EDS). The system has been used in conjunction with SEM since 1968 and has been making use of solid-state detectors for measuring X-rays [36]. SEM has been developing with the advent of modern equipment. Danilatos studied the effect of the environment on analyzed samples during 1991-1993, which led to the development of an environmental scanning electron microscope (ESEM) for examining the surface of a specimen, whether it is dry or wet [38,39]. Among these advancements in SEM, the most recent one is the generation of digital images, which are then displayed on computers for analysis. At present, the majority of the SEM instruments have modern software, for analyzing obtained data, and EDS system, which makes the use of computer programming for evaluating the composition of various elements present in the sample [36]. The use of modern software provides improved quantitative analysis and converts the X-ray intensity into chemical compositions of the sample, in a relatively shorter period of time.

1.2. Basic SEM Operation

The typical energies of incident electrons coming from electron guns in SEM, in general range from 2 keV to 40 keV [11]. The SEM instrument can be classified based on the range of energies, which is subject to the type and nature of samples and analyses, such as low voltage SEM, standard SEM, high-resolution SEM, and field emission SEM. Electron guns are also chosen based on the intended application, and there are three types of electron guns usually used for SEM. Type one is the tungsten filament electron gun, which is heated over 2500°C resulting in the thermal emission of electrons from its tip [40,41]. The second type of electron gun is lanthanum hexaboride filament which produces thermionic emissions, with the advantages of longer work-life time and a brighter beam of electrons from a larger maximum beam current [42,43]. These electron guns are relatively more expensive than the conventional tungsten filament ones. Field emission guns are the third type of electron guns, and are known as cold cathode electron emitters, as heating is not involved in the process [44,45]. It works with the application of a very high electric field to a finely pointed tip, which results in providing the brightest beam with a very small deviation in electron energy. Since the field emission guns need 10^{-10} torr pressure for preserving the tip, the cost of SEM with these guns becomes expensive [11].

The electron beam is demagnified into a fine probe by two or three electromagnetic condenser lenses. Scan coils are used with fine probes for scanning across the selected surface area of the specimen. The electrons coming from the probe penetrate into the sample in a tear-dropped-shape volume (

). The overall dimensions of this volume are determined by various factors such as the electron beam energy and the atomic masses of the constituent elements present in the specimen. Higher energy and lighter atomic masses of elements tend to result in increased penetration depth inside the sample. The angle of incidence does not significantly affect the penetration depth, rather it affects the angle of deflection, scattering, and other electron interactions as the beam traverses through the specimen. The production of secondary, Auger, and backscattered electrons takes place due to the interaction of the electron beam with the sample surface. It also accompanies the production of characteristic, continuum, and fluorescent X-rays (

 doi:10.20944/preprints202310.2059.v1

).

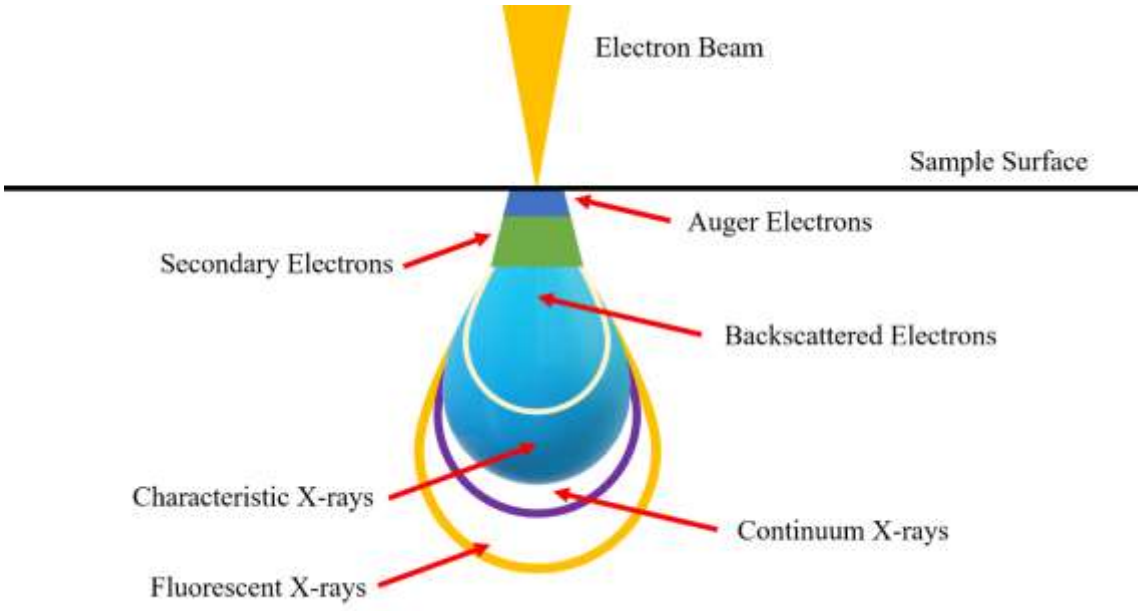

Figure 2. Various levels of electron penetration through the sample surface.

The elastic interaction between an electron beam and the sample results in electrons reflecting back, termed as backscattered electrons (

). These electrons are used for generating high-resolution images of the constituent elements present in the specimen. The inelastic collision results in relatively lower energy electrons originating from the atoms of the sample, are known as secondary electrons, and are helpful in investigating the topography of the specimen surface. Auger electrons are emitted when excited atoms release energy and are characteristic of the sample elements. These electrons help in understanding the elemental composition of the specimen. When the electron beam displaces an electron from the inner shell of an atom, another electron from a higher valence shell takes its place, resulting in a small loss of energy in the form of an X-ray photon. It is considered a characteristic X-ray and helps in investigating the particular element from which it is emitted. The electrostatic force experienced by the high-energy incident electron beam due to the presence of atomic nuclei, results in deflections/accelerations/decelerations of electrons. This results in the production of continuum X-rays (also known as Bremsstrahlung or Brems X-rays) having a continuous spectrum ranging from low to high energies (

). The continuum X-rays do not contribute towards primary elemental analysis; however, they help in studying the interaction between the sample and the electron beam. Fluorescent X-rays are a subset of characteristic X-rays, resulting from the filling up of the inner shell by outer shell electrons (

). Characteristic X-rays are emitted from the vacancy left by an ejected inner-shell electron, while fluorescent X-rays are produced when the outer-shell electron fills the vacancy. Fluorescent X-rays contribute valuable information about elemental information in addition to the main characteristic X-rays. They also help in studying the background radiation in the X-ray spectrum [11] (**Error! Reference source not found.**).

The signals of this electron and X-ray production are collected by various detectors present in the specimen chamber of SEM. A monitor is fed with the signals from each detector, and a rectangular pattern of parallel scanning lines is synchronized with the electron beam [11]. The field emission gun SEM (FEG-SEM) can produce high-resolution secondary electron images, owing to the intense electron beam, and is capable of achieving sub-nanometer to nanometer-scale resolutions [46].

 doi:10.20944/preprints202310.2059.v1

It is important to understand the meaning of magnification value in SEM images. In general, the magnification value provides information about the size ratio in between the actual and the enlarged image of specimen. SEM produces high-resolution images for visualizing the material surfaces. During the imaging process, the level of enlargement applied to the specimen is given by the magnified value of the SEM image. This magnification is usually expressed as a numerical value (such as 1,000x, or 10,000x) visualizing how many times larger the imaged structures or features are shown, as compared to the actual sample. It is one of the fundamental features of SEM to have the ability to control magnification. The level of magnification can be adjusted to have an overview of the specimen's surface structure or to focus on any specific structural details. **Error! Reference source not found.** shows ilmenite micrographs having various magnification levels, aimed to analyze the existing (a) cracks, (b) furrows, and (c) particle shape in the sample [47].

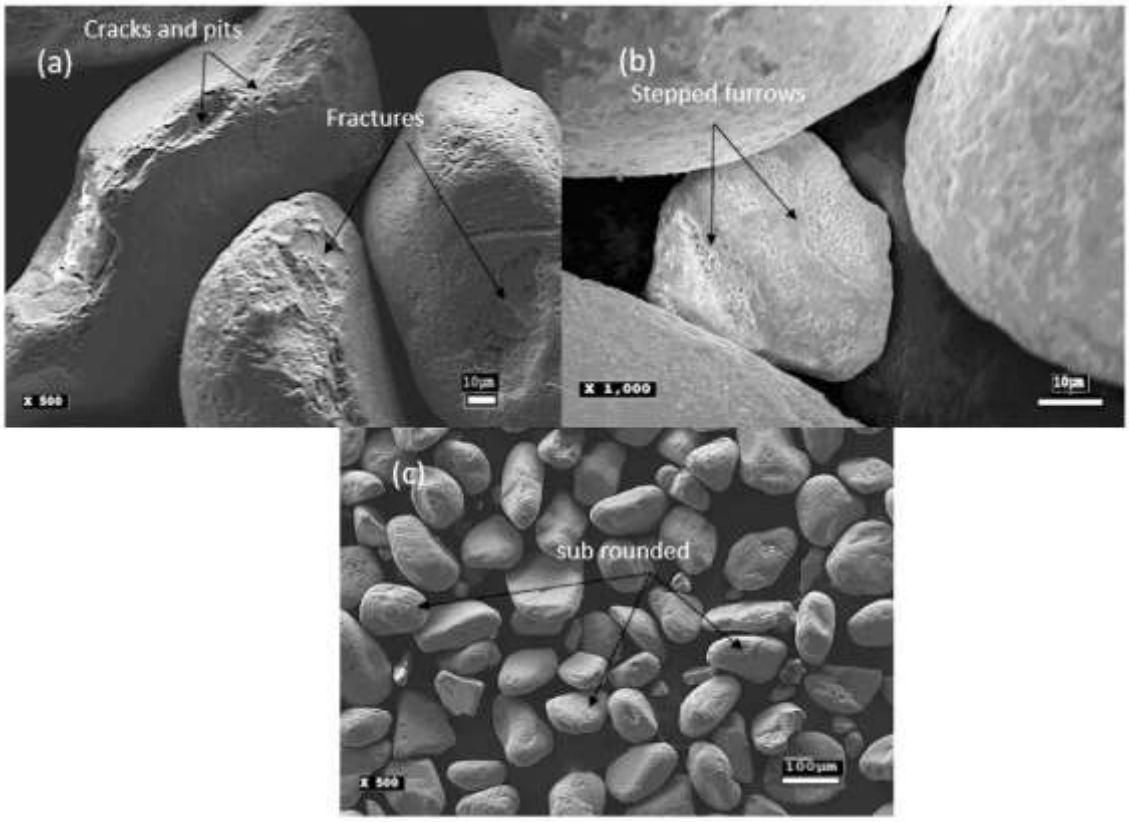

Figure 3. Ilmenite micrographs having various magnification levels, aimed to analyze the existing (a) cracks, (b) furrows, and (c) particle shape in the sample [47]. CC-BY.

1.2.1. Specimen Preparation

For the production of high-quality and accurate SEM images, the sample preparation stage is very important. The SEM analysis is susceptible to distortions, artifacts, and other issues in case of improper specimen preparation. The sample of interest can be a solid material, a biological specimen, or belonging to any other area of the object to be analyzed. The specimen material is mounted on a stub or holder using an adhesive conducting double-sided tape or with other mounting techniques. The SEM stubs are electrically conducting pads. No special specimen preparation is required for conductor or semiconductor materials. For insulator materials, the image is distorted by charging the sample, and therefore a conduction path to the ground is required for clear image production [11]. If the sample is moist, it is ensured that the sample is completely dry before going into the SEM analysis stage. The moisture can introduce charging effects thereby distorting the quality of the image. For materials of interest without or with lower electrical conductivity, a thin coating of metals such as gold, platinum, palladium, and chromium is applied to prevent charging effects [48–50]. Samples can

 doi:10.20944/preprints202310.2059.v1

be trimmed, fractured, or cut to the expose the surface of interest to the electron beam, and to make the geometry and size of the sample suitable for SEM analysis.

 doi:10.20944/preprints202310.2059.v1

1.2.2. Imaging Process in the SEM

The SEM images are formed by using various signals (

) collected by the detectors, present in the collection chamber. Each signal offers different types of imaging information for the sample [11]. Secondary electron imaging (SEI) is an extensively utilized imaging mode in SEM, which produces images by detecting secondary electrons [51]. It provides topographic information such as surface textures, shapes, and features. Backscattered electron imaging (BSEI) is generated by detecting backscattered electrons coming from the surface of the sample due to interaction with the primary electron beam [52].

BSE images indicate compositional contrast, with respect to the atomic number of the elements present in the sample (**Error! Reference source not found.**). This atomic number contrast provides tremendous value in detecting elements in the samples containing a variety of chemical compositions. Elements with higher atomic numbers appear brighter in BSE images, while darker appearance represents the elements having lower atomic numbers [53–56]. This feature is especially helpful for mineralogists and geologists as it allows the identification of various mineral phases present in a rock sample. BSE provides value in analyzing the sample surface topography by showing surface texture, morphology, and roughness, which may not be clear in secondary electron images. Certain features of the sample can be studied by BSE contrast enhancement, as it allows characterization of subtle compositional variations. BSE imaging is also helpful in studying the non-conductive elements, which is not the case with secondary electron images. BSE imaging can also be coupled with other diffraction and spectroscopy techniques, such as electron backscatter diffraction (EBD) for analyzing the crystallographic properties of materials at a granular level, and with energy-dispersive X-ray spectroscopy (EDS) for quantitative mapping of elemental distributions.

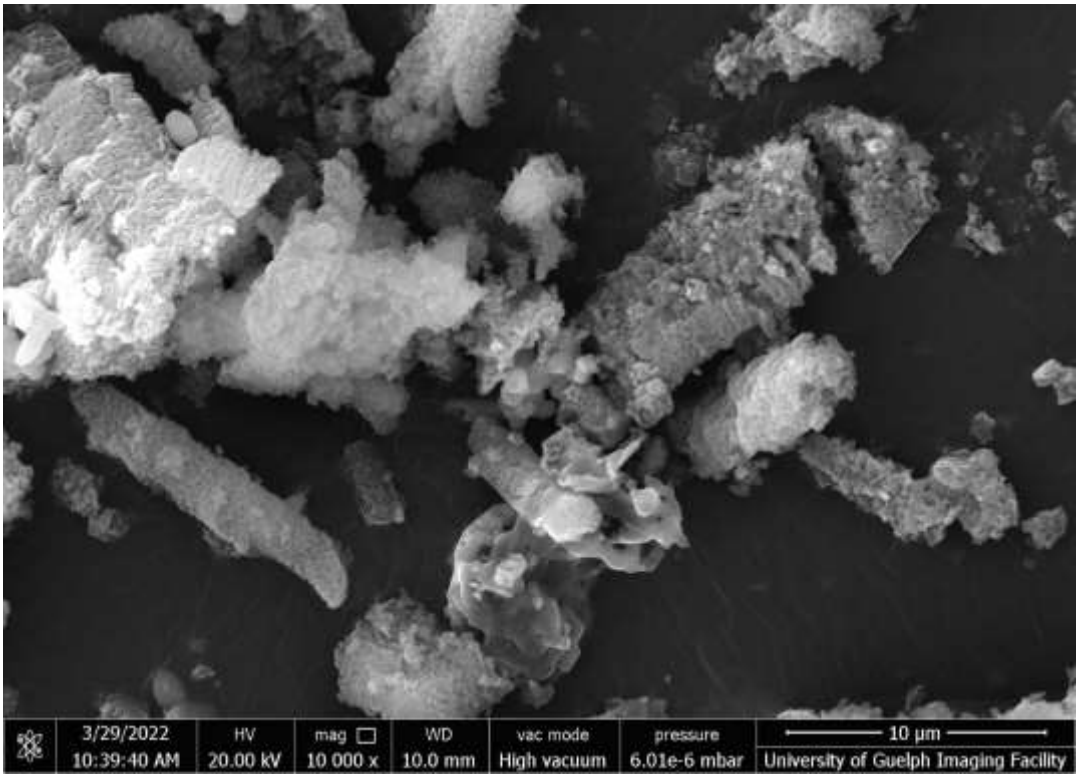

Figure 4. BSE image of some minerals retrieved from a leaching investigation.

When high-energy electrons coincide with the sample, some materials have the tendency to emit light, imaging that signal is considered as cathodoluminescence imaging (CLI) [57]. The luminescent properties and defects of the sample material are revealed by CLI images. The electrical properties of materials are studied by using the electron beam-induced current (EBIC) technique [58]. It is specially used for semiconductor materials with localized charge carriers. Electron-hole pair in a

 doi:10.20944/preprints202310.2059.v1

semiconductor material is created with the help of the primary electron beam. With the application of external voltage, the created charge carriers start moving in response to the acting electrical field, indicating a measurable current, which is used to investigate the electrical properties of materials. This technique is also valuable in the identification of defects, grain boundaries, and other microstructural features affecting electrical behaviors. The electrical functionality of semiconductor devices is studied with the aid of voltage contrast imaging (VCI), which indicates the variations in electrical potential or voltage across the surface of the specimen [59].

1.3. Fundamental Theoretical Calculations

Crewe et al. in 1969 demonstrated the basic theoretical calculations that were helpful in the designing and selection process of SEM [60]. Their work helped in identifying the correct probe size for SEM. The aberrations of diffraction and electron gun, as well as the first order image of the field emission tip aid in determining the size of examining SEM probe at the specimen. The diameter (d_s) of an effective source leads toward an image with the following correlation:

$$d_s = 2mR\left(\frac{\overline{v_T}}{v_1}\right)^{1/2} \quad (1)$$

where m is the magnification of the gun, R represents the actual radius of the tip, $\overline{v_T}$ indicates the average transverse energy of electrons coming out of the tip (~0.2 V), and v_1 is the emission voltage required to produce 1 μamp emission current. The term $\left(\frac{\overline{v_T}}{v_1}\right)^{1/2}$ is the characteristic of a field emission source and indicates the reduction factor of effective source size.

The theoretical spot size is affected by the aberrations of the gun with the following two terms:

$$d_a = \frac{mC_s\alpha_1^3}{2} \quad (2)$$

$$d_c = mC_c\alpha_1\Delta V \quad (3)$$

where d_a is spherical aberration, d_c is chromatic aberration, C_s is the spherical aberration constant, C_c indicates the chromatic aberration constant, $\alpha_1$is the entrance half angle of electron bean, and ΔV represents the total energy spread of electrons. ΔV is maintained such that the total energy spread of electrons leaving the tip remains 0.2V, while variations in V_0 and V_1 can be considered negligible [60].

At the defining aperture, the diffraction effect should be included. The diffraction contribution to the final spot size (d_d) can be calculated as follows:

$$d_d = \frac{0.6m\lambda_1}{\alpha_1} \quad (4)$$

λ_1 represents the electron wavelength at the first anode. The focused spot diameter can be estimated by combining the four terms as follows [60]:

$$d_{rms} = \sqrt{d_s^2 + d_a^2 + d_c^2 + d_d^2} \quad (5)$$

2. Scanning Electron Microscopy and Mineral Characterization

SEM makes use of secondary electron imaging to analyze the surface topology and morphology of micron/nanometer scale minerals [61]. For a comprehensive understanding of microstructure and mineral components, the SEM method is usually combined with X-ray techniques to complement the acquired information [62–65]. The infrared spectroscopy method is helpful in identifying chemical species and determining the molecular structure of the minerals. This technique has been widely used in mineral characterization [66–69].

One of the major quantitative analysis methods in mineral analysis is X-ray diffraction (XRD). It correlates the content of minerals with diffraction density, which helps in identifying and quantifying

 doi:10.20944/preprints202310.2059.v1

the minerals present in the sample [70,71]. For example, XRD can be used to analyze the calcite and nahcolite in saline brine [72], to evaluate the deposit by identifying minerals in phyllite [73], to examine the order degree of dolomite [74] and study the content of calcite and dolomite in carbonate rocks [75]. XRD is a rapid and accurate method for quantitative mineral analysis, however, some mineral compositional structures could lead to errors in analytical results [70].

Combining the qualitative analysis with quantification assessment methods can provide a better understanding of the investigated minerals. Such methods include SEM energy dispersive spectroscopy (SEM-EDS) [75–78], automated SEM mineral liberation analysis (SEM-MLA) [79–81], and quantitative evaluation of minerals by scanning electron microscopy (QEMSCAN) [82–84]. These methods incorporate a mineral quantitative analysis system by an using energy spectrometer and SEM. For accurate identification of minerals, backscattered electron (BSE) images are used, which can reflect the difference between the X-ray energy spectrum and mineral phase composition [85–87]. The quantitative analysis of rare earth minerals is a challenging task with conventional identification methods, the above-mentioned techniques have attained the rare earth minerals identification. The problems in the usage of these methods pertain to the difficulty in application, promotion, and high measurement cost.

2.1. SEM Energy Dispersive X-Ray Spectroscopy (SEM-EDS)

When the electron beam, emitted from the gun, penetrates and interacts with the volume beneath the sample surface, X-rays are generated. This is a well-established principle in physics, the deceleration of electrons due to their entrance in the Coulomb field of specimen, results in loss of electron energy and emits photons. In SEM analysis, similar X-ray photons are emitted which are characteristic of the sample under investigation [85], as shown in

.

The quantification scheme is delivered by measuring the X-ray intensity. This was illustrated by Heinrich and Yakowitz in 1968 in their publication namely, Quantitative Electron Probe Microanalysis [88], which later became the standard for developing X-ray fields. At that time, X-ray absorption, determination of correction factors at the instant of electron penetration and scattering, and conversion of X-ray intensity to the relative concentration were missing. Many problems pertaining to the electron probe field were solved with the development of energy dispersive spectrometry (EDS). At present, various studies have incorporated SEM-EDS for qualitative and semi-quantitative analysis in a variety of subject areas [89–95].

The schematic diagram of the energy dispersive spectrometer is shown in **Error! Reference source not found.**. The X-ray detecting system (which is a solid-state detector) separates the characteristic X-rays of various elements present in the sample. Then the EDS system software analyzes the energy spectrum to determine the amplitude of particular elements, and electrical signals are generated from respective photon energy. This results in qualitative and quantitative determination of chemical composition maps of the elements present in the sample [85]. SEM-EDS have been used in a variety of fields for mineral characterization [96–102].

 doi:10.20944/preprints202310.2059.v1

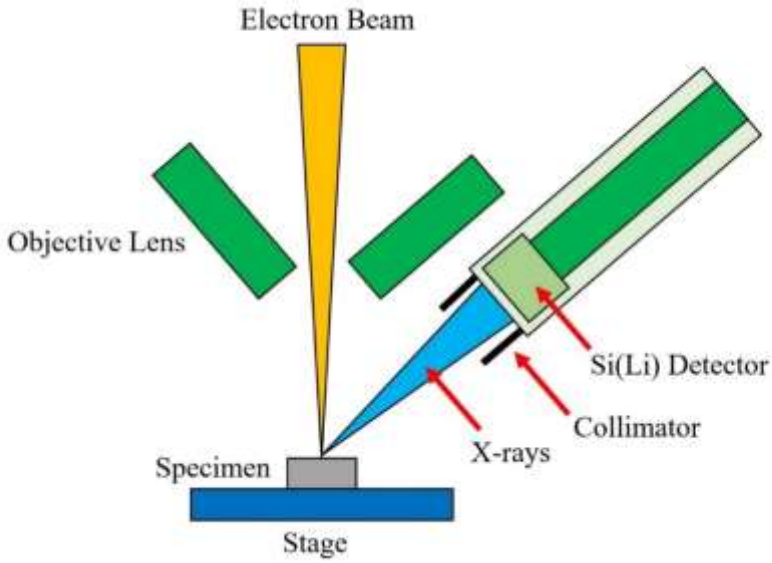

Figure 5. Schematic diagram of energy dispersive spectrometer.

2.2. SEM-Based Automated Mineralogy (SEM-AM)

SEM-AM is a tool that was initially designed to characterize mineral processing products and ores. The measurement process starts with collecting backscattered electron (BSE) images, which are analyzed with image analysis software procedures. Based on BSE image adjustments, the energy dispersive X-ray spectra (EDS) are gained at selected points. The EDS spectra of the sample is then classified based on the list of approved reference EDS spectra. Relevant software providers offer services such as particle analysis, EDS spectral mapping, sparse phase search, and point counting modal analysis using four principal SEM-AM measurement routines and different classification algorithms, which can be used based on the analysis requirement. The main challenges of the process are materials with very different hardness, polishing of relief surfaces in particles, and electron beam stability and appropriate non-evaporating epoxy resin mixtures [80].

SEM-based automated mineralogy (SEM-AM) is still under-utilized, despite the fact that SEM instruments are widely distributed in industry, geosciences, and material research. SEM-AM can produce valuable results in a variety of major applications by characterizing the primary ores, and optimizing the mineral concentration, flotation, comminution, and metallurgical processes in the mining industry with the generation of quantified reliable data [103–107]. Beyond the classical fields, the potential of SEM-AM gains further interest on scientific and economic grounds. Some closely related topics are ore fingerprinting, metallurgy, and applications in petrology [108–110].

SEM-AM systems are a combination of hardware platforms, processing software, and specific image analysis. Any SEM with minor adjustments can be used as a hardware tool for SEM-AM. These adjustments include a high-vacuum operation mode and additional internal mainboards. The vacuum pressure of 10^{-5} to 10^{-7} Pa is required for its operation. The electron source of Tungsten cathodes and field emission guns can be employed. Tungsten cathodes can be used for economical operation; however, field emission guns are recommended for long-term stability of electron beams for automated measurements. The speed of analysis and the X-ray count rate are increased in SEM-AM by employing two or more EDS spectrometers in the SEM hardware. Multiple samples can be accommodated in a large sample chamber for simultaneous analysis in a single measurement session. A very accurate stage movement of SEM allows precise positioning using small intervals. For valuable analysis results, a fine-quality backscattered electron (BSE) detector is required. In SEM-AM analysis, BSE image quality and BSE image stability are important factors, as the resultant image (in combination with the EDS spectrum) is used for phase or mineral discrimination. Prior to the measurement, fixed working distances must be set to allow constant BSE image grey levels [80].

 doi:10.20944/preprints202310.2059.v1

Keeping the image calibration constant makes sure that a specific phase or mineral always possesses the same BSE image grey level. The calibration process can be conducted with various BSE image grey levels of reference materials such as quartz (dark grey), copper (intermediate), and gold (very bright) [80]. A choice of calibration reference materials should be made based on the sample materials to be investigated. For example, many slags, industrial ashes, or particulate materials are investigated using SEM-AM, and quartz or copper are used for calibration with BSE image grey levels of dark grey to intermediate. This results in SEM images with better resolution and quality. For SEM-AM technology, four principal measurement routines can be outlined, which starts with collecting BSE grey-level image with respect to the calibrated grey level, as shown in **Error! Reference source not found.**. The upper row represents the BSE images, while the bottom row indicates the EDS images of SEM-AM one measurement frame. White or black crosses denote the points of X-ray analyses (only some points are shown). **Error! Reference source not found.** represents the EDS point counting technique used for the quantification of modal composition. **Error! Reference source not found.** indicates particle analysis by EDS, which has been developed for fast automated characterization of grain mounts with up to 10^6 particles, such as milled products from mineral processing and mining. **Error! Reference source not found.** denotes the sparse phase search method, which combines single spot EDS spectral analysis of grains with a BSE grey tone value trigger. It is valuable in massive rock applications, such as drill cores and in thin sections. **Error! Reference source not found.** expresses EDS spectral mapping which combines BSE image levels with the mapping of EDS spectrum. This method is helpful, especially in cases where fine details of mineral intergrowth are considered. In summary, SEM-AM is a powerful tool for mineral characterization and has actively been used in recent literature [111–113].

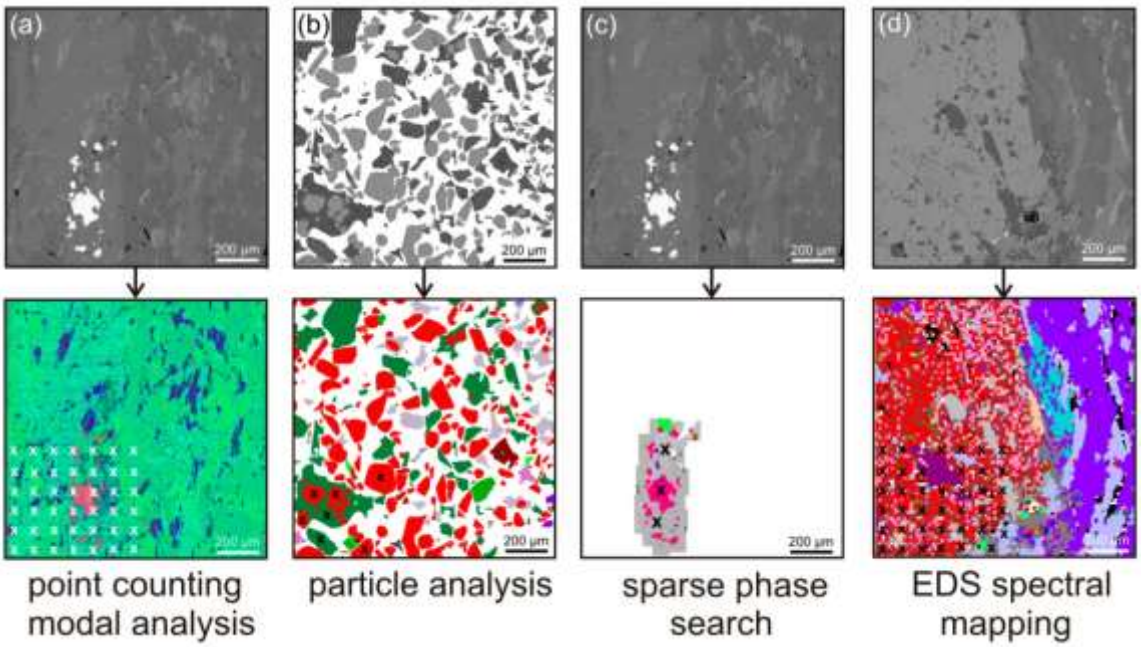

Figure 6. SEM-AM methods of one measurement frame showing BSE (upper row) and EDS (lower row) images. Numerous single EDS analysis points map each grain with a distinguishable BSE grey level and visualized as color-coded pixels, such as the garnet grain is indicated by red-colored pixels [80]. CC-BY.

2.3. Automated SEM Mineral Liberation Analysis (SEM-MLA)

Recent software developments in SEM have incited a dominant growth in applications of solid matter investigations. One of the economic solutions is the use of mineral liberation analysis (MLA) for optimizing the mineral processing methodology of metallic ores. SEM-MLA has been an important drive for transforming numerous software versions of SEM applications [80]. SEM-MLA

 doi:10.20944/preprints202310.2059.v1

was designed to quantify the mineralogy of ores. After the mining process, the ore is processed to increase the concentration of minerals of interest (and value). The processing of the ore is also important for removing minerals of no value or those having detrimental effects on the required mineral products. This processing of grinding the ore and liberating the mineral of interest provided rapid automated analysis of target minerals and extensively improved the process.

Mineral liberation analyzer (MLA) based on SEM was developed in the late 1990s by the JKRMC (Julius Kruttschnitt Mineral Research Centre, Australia) and it is commercially available now [114]. In MLA, minerals are differentiated by attaining and combining the information gathered from the EDS and BSE. Depending on the size range of particles in the sample, size fractions from the samples are produced. Then liberation is measured in each size fraction, followed by the liberation reconstruction of the whole sample. The measurement of mineral liberation is usually carried out through one of the two methods, i.e., either the area method or the linear intercept method. Liberation by area measurements has shown lower stereological error as compared to the linear measurements.

It is important to note that the liberation measurements by linear intercepts are known as one-dimensional, while the area method ones are called two-dimensional liberation. Both of the measured liberations are lower dimensional projections of the true volumetric liberation (which is three-dimensional). Stereological correction is based on the stereological transformation and prediction of liberation measurements. This stereological correction can be based on entropy regularization [115]. The correction of the apparent liberation and the production of three-dimensional liberation have also been described in several other investigations [116–118]. Various operating modes for the MLA system are available, i.e., X-ray modal analysis (XMOD), particle X-ray mapping (PXMAP), selected particle X-ray mapping (SXMAP), sparse phase liberation analysis (SPL), standard BSE liberation analysis (BSE), extended BSE liberation analysis (XBSE), and rare phase search (RPS) [119]. The use of SEM-MLA is shown in **Error! Reference source not found.**, for quantifying the mineralogy of a hydrothermally overprinted alkali plutonite [81].

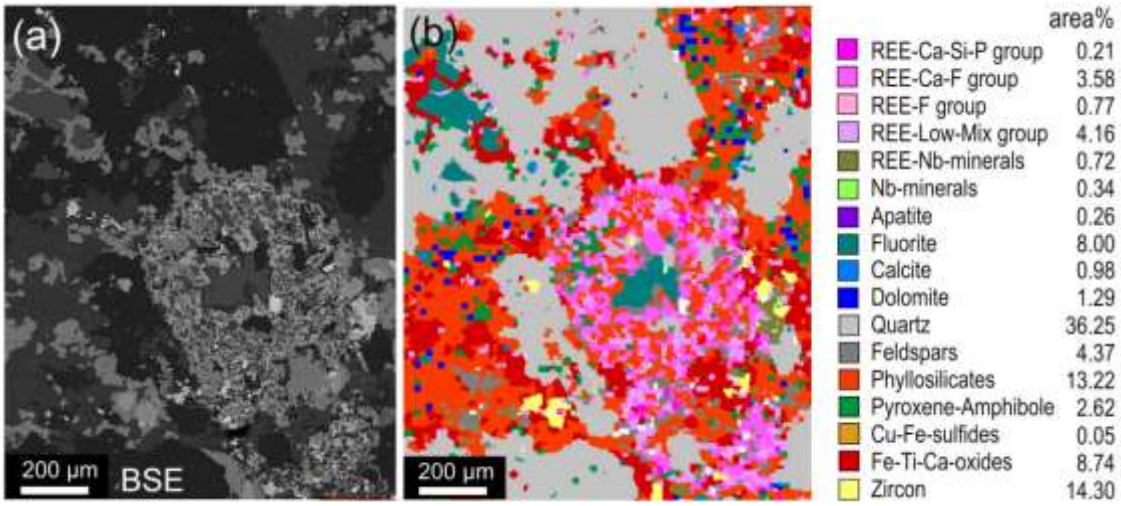

Figure 7. (a) SEM-MLA measurement of a hydrothermally overprinted alkali plutonite showing backscattered electron (BSE) image (b) Color-coded, grouped, and classified presentation of frame present in (a) [81]. CC-BY.

2.4. Quantitative Evaluation of Minerals by Scanning Electron Microscopy (QEMSCAN)

Traditional mineral analysis based on microscopy could not provide the required data because of the absence of quantitative information and the very small size of the particles of interest. QEMSCAN technology, initially termed QEM*SEM, demonstrated the potential of revolutionizing automated mineralogy [120]. In a mold, the particulate mineral sample is mixed with epoxy resin, and the sample surface is prepared using cutting, polishing, and carbon coating. The sample is

 doi:10.20944/preprints202310.2059.v1

scanned using SEM in backscatter mode, enabling the differentiation of particles with the background. After the identification of particles on the resin block, their composition is systematically mapped using EDS. In contrast to the most modern SEMs containing single EDX, QEMSCAN possesses the attribute of having multiple EDX at the same time, enabling rapid quantitative mineralogy. The acquired EDX signals are then compared with reference known materials in the database and assigned a mineral name or to a chemical compositional grouping. With this process, the mineralogy of the sample can be conducted, particle by particle, analysis by analysis [120]. QEMSCAN locates the particles using a BSE signal, while identifying the mineral by an EDS signal. It can be compared to the SEM-MLA which makes more use of the BSE signal than EDS one for identifying the mineral. SEM-MLA works very well for bright phases (such as platinum group element minerals).

Among SEM-EDS techniques, QEMSCAN is one of the most widely used, which offers quantitative characterization of minerals, ores, and other mineralogical compounds [121–125]. QEMSCAN is usually used in conjunction with other analytical techniques such as electron probe microanalysis (EPMA) and X-ray diffraction (XRD), as shown in **Error! Reference source not found.** [126]. **Error! Reference source not found.** indicates the use of QEMSCAN for identifying the mineral distribution of four samples [126]. It shows the presence of geothite, quartz, clay, limonite, and other silicate minerals.

Table 1. Techniques used for investigating mineralogy and their comparison. ✓ indicates good, ● represents poor, while (✓) suggests it is possible but not recommended [126].

Investigation	Electron microprobe	XRD	QEMSCAN
Mineral textures	(✓)	●	✓✓✓
Mineral distributions and associations	(✓)	●	✓✓
Mineral specific particle size information	(✓)	●	✓✓
Mineral abundances	●	✓✓✓	✓✓✓
Amorphous minerals (geothite, silica)	✓✓✓	●	✓✓✓
Distribution of minor metals within minerals	✓✓✓	●	✓
Crystallinity (clays, silica, geothite, and limonite)	●	✓✓✓	●

 doi:10.20944/preprints202310.2059.v1

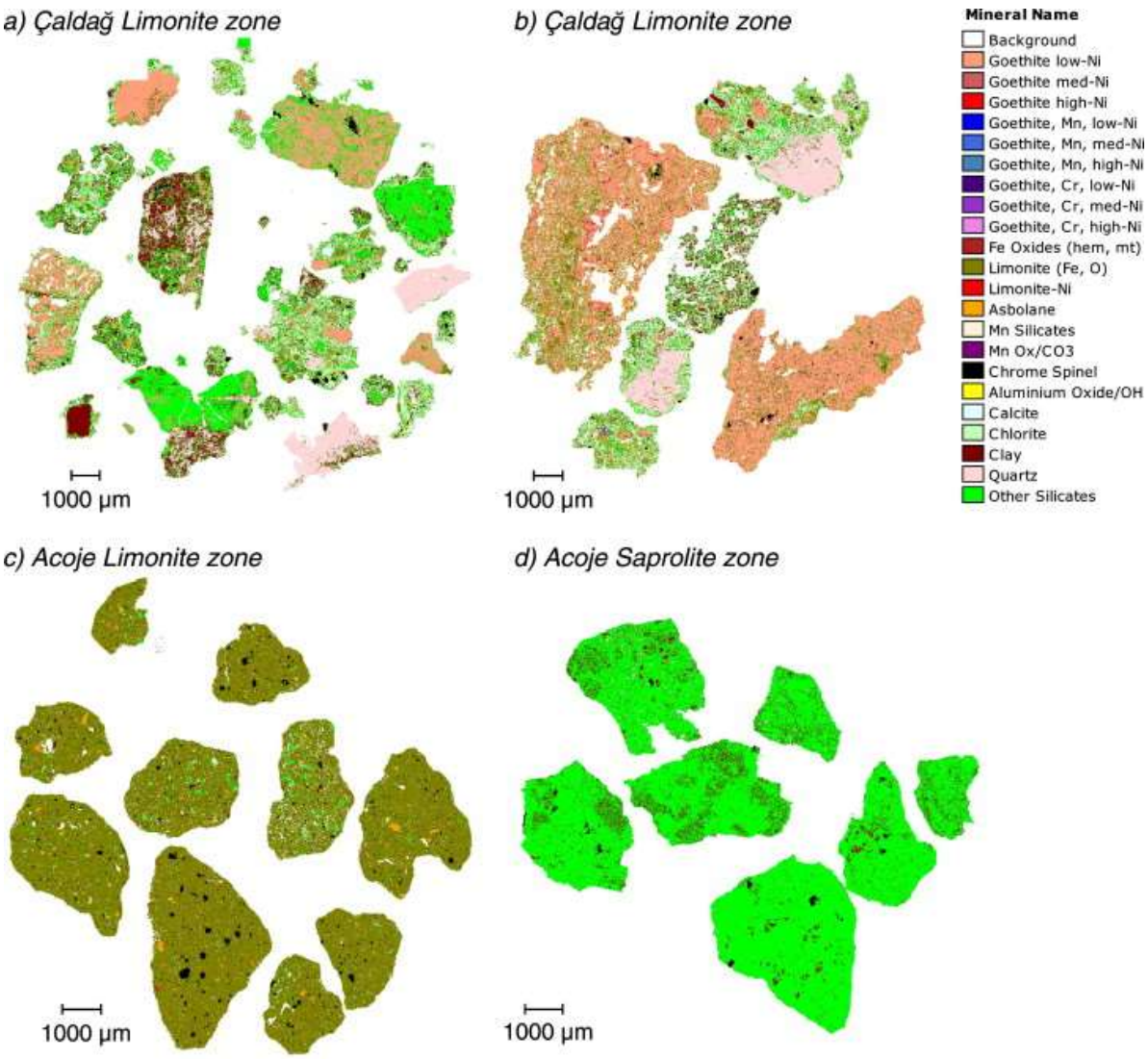

Figure 8. QEMSCAN analysis indicating mineral distribution in four different zones [126]. CC-BY.

The above-described four analytical techniques are distinct but complement each other in comprehensive mineralogical analysis. High-resolution images are provided by SEM, elemental composition analysis is provided by EDS, while SEM with automated mineralogy involves a thorough mineral characterization. Most of the SEM with automated mineralogy equipment use have EDS incorporated, where software utilization provides objective and quick mineral characterization and other analytical results. QEMSCAN is a specific instance of the broader concept of automated mineralogy, which represents a specific system and brand used for comprehensive mineral characterization. MLA systems are used in geology, mining, and mineral analyses for ore processing and beneficiation, as they provide insights into the degree of liberation of valuable minerals from the host rock. Combining these techniques together offers constructive value to the mineral characterization and analysis process, by not only providing high-resolution surface images, but also offering the elemental composition of the samples, the degree of liberation of minerals, and saving time in determining the presence of valuable minerals present in the ores. In short, SEM demonstrates itself as a powerful technique for the characterization and analysis of various minerals [127–129].

Mineral characterization is usually carried out with more than one technique, for clear identification and quantification. Therefore, the SEM analysis for mineral characterization is accompanied by several other analytical techniques, as mentioned in **Error! Reference source not found.**, which have been applied in some of the recent publications.

 doi:10.20944/preprints202310.2059.v1

Table 2. Recent SEM applications focusing on mineral identification, quantification, and characterization.

Analytical Methods / Techniques	Year	Minerals / Materials	Reference
SEM/SDD-EDS, EPMA-WDS,	2023	Major and minor elements in minerals and rocks	[130]
SEM-EDS, XRD	2022	Constituent minerals in shales	[131]
SEM, TEM	2018	Microbial biofilms, Mineral precipitation	[132]
SEM-BSE, TMR, SMH	2018	Mineral content in enamel lesions	[133]
SEM, μXRF, LWIR, SAM	2020	Quartz, olivine, kyanite, diopside	[134]
SEM-EDS, Raman Spectroscopy	2019	Asbestos	[135]
SEM-EDX, XPS, XRD, FT-IR, UV	2020	Kaolin, Illite, Gibbsite, Quartz	[136]
SEM, XRD, TGA, IR, TXRF	2022	Mineral constituents in human renal calculi	[137]
SEM-FIB	2021	Mineralized bone	[138]
SEM-EDS	2021	Mineralizing fluids, sedimentary brines	[139]
SEM-FIB, μCT, XLH	2020	Crossfibrillar mineral tessellation	[140]
SEM, BSE, EDS,	2022	Sandstones	[141]
SEM, CT, Raman Spectroscopy	2021	Saturated brine, wellbore cement	[142]
SEM-EDS, XRD, IRS, XRF	2023	Gabbro-anorthosite, seawater, mafic rock	[143]
SEM-EDS, AM-SEM, FE-SEM, CT	2023	Mineralogical analysis of petroleum geology	[144]
SEM-FIB	2020	Mineralized scale patterns on the cell periphery	[145]
SEM, EMP, Raman Spectroscopy, BSE	2019	Petrified wood, Mn-oxide minerals	[146]
SEM-EDS, Monte Carlo Simulations	2021	Glass fibre-reinforced cement	[147]
SEM, XRD, XRF, FTIR	2022	High ash coal, fluidized bed gasifier	[148]
SEM-EDS, XRD	2023	Mineral-forming bacteria	[149]
SEM-EDS, XRD, TGA	2023	Self-healing cement-based minerals	[150]
SEM, XRD, XPS, FTIR	2023	Biomimetic mineralized cement	[151]
SEM, TEM, PLM, EBSD, SAED	2023	Talc, amphiboles, biopyriboles	[152]

Where, SEM = Scanning Electron Microscopy, SDD = Silicon Drift Detector, EDS = Energy Dispersive X-Ray Spectroscopy, EPMA = Electron Probe X-Ray Microanalyzer, WDS = Wavelength Dispersive Method, XRD = X-Ray Diffraction, TEM = Transmission Electron Microscopy, BSE = Back-Scattered Emission, TMR = Transverse Micro-Radiography, SMH = Surface Micro-Hardness, μXRF = Micro X-Ray Fluorescence, LWIR = Long Wave Infrared, SAM = Spectral Angle Mapper, EDX = Energy Dispersive X-Ray Spectroscopy, XPS = X-Ray Photoelectron Spectroscopy, FT-IR = Fourier Transform-Infrared Spectroscopy, UV = Ultraviolet Visible, TGA = Thermogravimetric Analysis, TXRF = Total Reflection X-Ray Fluorescence, FIB = Focus In Beam, μCT = X-Ray Micro-Computed Tomography, XLH = X-Lined Hypophosphatemia, IRS = Infrared Spectrometry, AM = Automated Mineralogy, FE = Field Emission, EMP = Electron Microprobe, PLM = Polarized Light Microscopy, EBSD = Electron Backscatter Diffraction, SAED = Selected Area Electron Diffraction.

 doi:10.20944/preprints202310.2059.v1

3. Uncertainties in SEM Measurements

The advancement of SEM with automated mineralogy has provided a quick and relatively economical quantitative mineral analysis solution. However, the absence of statistical errors makes the robustness of the results uncertain. This could damage the reliability of the technical solutions taken on the onus of these quantitative outcomes [153]. The automated mineralogy-based measurements have been studied with several methods for the estimation of uncertainties. For instance, a statistical approach was developed by Benvie et al. in 2013, for using SEM automated mineralogy in accordance with the diagnostic leaching tests [154]. It was concluded that, for deriving the standard deviation and the background variance, at least two-grain mount measurements were required for each head and leach residue sample. In another study, the variability in mineral liberation analyses and mineral quantity was investigated by Lastra and Paktunc in 2016 [155]. They studied a fraction of sulfide flotation rougher concentrate of -509 to 208 μm size through inter-laboratory testing. It was found that mineral quantities are having good agreement with the data, but mineral association and liberation analyses showed less agreement. It portrays a hint towards the idea that it is not necessary that correct mineral liberation and association can be found with correct mineral quantities. Guseva et al. in 2021 evaluated analytical errors in mineralogical measurements by applying the point counting method via binomial distribution approximation [156]. It came out that binomial approximation may not fit well with all the cases, especially with coarse materials, and other methods more suitable to the case should be used, such as the estimation of the confidence method [157] or bootstrap resampling method [158].

The estimation of errors in textural characteristics measured by automated mineralogy can be identified efficiently with the bootstrap resampling method [159]. For instance, the bootstrap approach can help in evaluating the uncertainties related to particle properties measured by SEM automated mineralogy for the evaluation of magnetic separation efficiency [160,161], density separation processes [162], and the simulation and statistical modeling of mechanical separation processes [163]. The bootstrap resampling method considers a population of N samples, takes M random subsets and replaces the randomly selected samples in order to make sure that the entire population is available for sampling [164,165]. The accepted statistical methods which use the point counting method on polished sections and assess errors in mineral grades, agree well with this bootstrap method [166–168]. This method has the advantage of being assumption-free and can be applied to a wide range of particle characteristics [158]. It does not assume a bionomical distribution. These methods imply that the standard deviation of mineral grades is proportional to the square root of the number of particles measured, or the total area of particles measured. The relative standard deviation of measurements for any mineral grade can be estimated as follows [169]:

$$RSD = ax^{-0.5} \quad (6)$$

Where, RSD is the relative standard deviation, a is a coefficient, and x is the mineral grade. The bootstrap method can also provide information about the measurement of how much total area (grains) to reach a given uncertainty. In addition to the uncertainty, SEM also has some drawbacks including, but not limited to, a limited depth of penetration majorly providing the surface information and low accelerating voltages providing low-resolution images, while increasing the voltage starts damaging the surface of the sample.

3.1. Constraints in Phase Identification by EDS Spectra

It is a common claim in SEM-based automated mineralogy studies that minerals can be detected, identified, and quantified by their characteristic EDS spectrum (an example is shown in **Error! Reference source not found.** indicating feldspar mineral albite [80]). However, this claim cannot be fully correct, as minerals are characterized by their lattice structure indicated by XRD first, and then comes the use of elemental composition information provided by EDS spectrum quantification. Therefore, mineral identification remains incomplete with the use of the EDS spectrum only, based on its foundations on elemental composition. Identifying a mineral with chemical composition alone can be misdirecting, as there are examples of minerals with similar chemical composition but

 doi:10.20944/preprints202310.2059.v1

different crystal structures, based on the crystallization conditions of minerals. For instance, pseudorutile and ilmenite, are titanium-iron oxide minerals, but both exhibit different crystal structures [80].

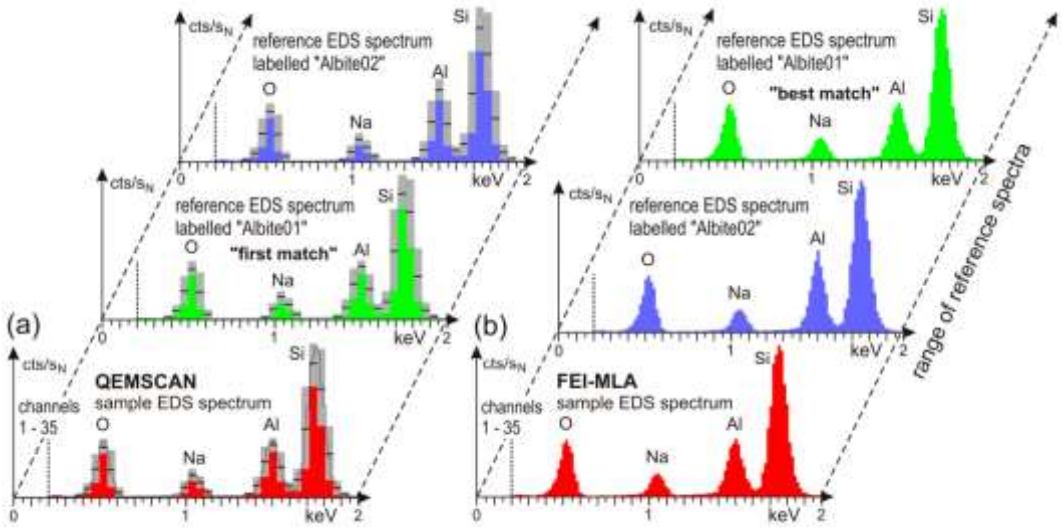

Figure 9. Classification modes of EDS Spectra (a) FEI-QEMSCAN (b) FEI-MLA for feldspar mineral albite [80]. CC-BY.

Another challenge to the mineral detection, identification, and distinguishing using EDS spectra is with minerals having very similar elemental composition, such as hematite (Fe_2O_3) and magnetite (Fe_3O_4). Hematite is composed of 70% by weight Fe and 30% by weight O, while magnetite is made up of 72% by weight Fe and 28% by weight O. The EDS spectra for both minerals appear to be very similar, and the very trivial differences in Fe and O peaks cannot be resolved apparently. In such scenarios, it is a good idea to use the BSE image grey level as an additional distinguishing standard. It must be noted that for such a measurement, a specific BSE brightness and contrast calibration is required. Another challenge is the detection range of EDS spectra, as it does not cover the whole elemental periodic system. For example, the first light elements cannot be detected by EDS, such as H, He, Li, and Be. It is, therefore, recommended to complement EDS spectra with XRD and XRF methodologies for mineral identification and quantification [80]. Some other the limitations of EDS spectra include longer mapping causing damage to the samples, low sensitivity of light elements, quantitative accuracy is not very high, information about the chemical composition only (not about functional groups or chemical bonds) and overlapping peaks making it difficult to distinguish among elements present in the sample.

3.2. Sample Preparation and Related Issues

For the success of any SEM analysis, an optimal sample preparation process is essential. A wide variety of samples can be analyzed using SEM. The configuration of the sample holder systems and the size of the SEM sample chamber are the defining parameters for choosing the type of samples for investigation. Grain mounts in round epoxy blocks are usually used for particulate or granular samples. If the samples are massive and compact matter, such as rocks, petrographic glass-mounted sections can be used. Depending on the type of the sample, the production of thin grain mounts on glass is also possible. Two important configurations must be maintained, whether it is samples on glass or round block sample holders i.e., the holder ought to be mounted perpendicular to the electron beam and parallel to the BSE detector [80].

 doi:10.20944/preprints202310.2059.v1

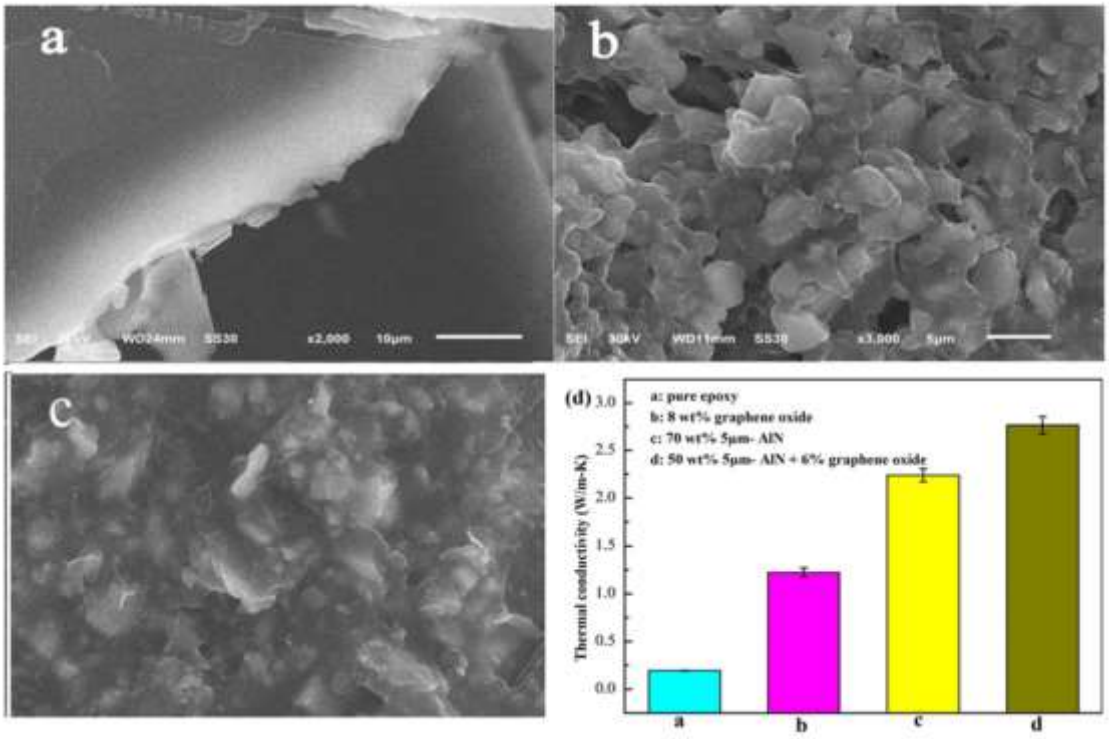

Figure 10. Epoxy adhesives shown using SEM having (a) epoxy resin only, (b) epoxy resin with aluminum nitride particles, (c) Epoxy resin with aluminum nitride and graphene oxide, and (d) Thermal conductivities of various test samples. CC-BY [170,175].

The grain mounts in epoxy blocks are the best form to prepare samples, if the sample material is non-compact, particulate, or granular matter, which can be ground, or hand-picked single, or broken grains [171]. A potential problem occurs when the grains are not easily separated with the same colored grey-scale BSE image, as most of the SEM-AM software packages are unable to distinguish between them. The use of pure graphite is beneficial in such cases, as it can be utilized in stirred form as a distance material into the epoxy resin blocks [171]. In some granular sample cases, a wide range of densities can exist among the phases present in the sample. With the stirring process of the sample grains with graphite-saturated epoxy resins, grains with larger size and high densities tend to move towards the bottom of the holding block, and it is more probable that the small grains will be missed from the analysis. One good practice for dealing with such kinds of samples is cutting the round blocks in vertical slices, which can be remounted as vertical sections [80]. It is also possible to study other materials such as polymers and coals, with the use of some EDS detectors. Since the BDE grey value of this organic matter is similar to the one of epoxy resin, an alternative embedding material should be used [172]. Carnauba wax is an alternative material that can be used for embedding in these cases [173]. Carnauba wax is a very soft material, which makes it difficult to be polished. One possible solution is to double-mount the Carnauba wax in epoxy resin blocks. Another prospective solution could be the doping of iodoform in epoxy resin [172,174]. The organic matter has, therefore, a lower atomic number than the epoxy resin, which makes epoxy to be considered as a background material. A wide variety of epoxy resins are available for this purpose [175]. The SEM images of some epoxy resins and their respective thermal conductivities are shown in **Error! Reference source not found.**. In addition to the variety, the proportions of the hardener and the filler can be varied. The challenges in choosing the epoxy resins are ones that remain stable under the 25 kV electron beam, which do not evaporate under high vacuum conditions, and which harden within convenient temperature conditions and time frames. The recommended ways of solving such problems are continuous application tests.

 doi:10.20944/preprints202310.2059.v1

The complication of the sample preparation procedure depends on the type of the sample material. If it is solid, dry, compact, and massive, the preparation of thin and thick sections is quite simple. In the case of brittle and/or porous material, epoxy resin is impregnated with a previous material for stabilization before sawing. Thin and thick section production has been reported by several studies [176–178]. Usually, silicon carbide SiC (with 600 to 1000 mesh) is used for lapping of the sample material behind the mounting on glass. In the standard lapping procedure, a SiC 1000 works best for brittle and soft materials, with a minimum substance loss, as compared to the SiC 600. If the sample contains minerals with different optical properties but a closer chemical composition, thin sections are advantageous, as an optical microscope can also be used to check the minerals and phases. Besides, the microscope with polarized light can be used for recognizing the samples with glassy phases owing to their optical isotropy. The reference EDS spectra list can be compiled based on this set of information [80].

A plane and well-polished surface is required for SEM-AM to analyze grain mounts of thin and thick sections and mounts in epoxy resins. Every material needs a specific treatment, so it is safe to state that the polishing part is a work of craftsmanship. In most cases, water is used in the polishing procedure. If there is a chance of water reacting or mixing with the minerals or materials, the sample preparation procedure can be carried out with water-free liquids such as ethylene glycol [80]. A variety of industrial ashes such as power plant and sewage ashes, can contain anhydrite, and the use of water-free liquids is recommended in such cases. For the samples having varying degrees of particles' hardness, the polishing plates covered with hard textile clothes are proposed. The plates with soft clothes having long fiber do work well for the samples containing minerals, soft metals, or ore minerals. The procedure of polishing the sample works well with decreasing grain sizes, for example, using abrasive papers first, then grinding, and then polishing powders on textile clothing. It is important to mention avoiding the use of lead-bearing polishing plates for general sample preparation, as it may cause sample contamination with lead. For the last step of sample polishing, the use of diamond powder with diamond paste or lubricant is very effective. The polishing procedure can be controlled using a reflected light microscope for inspecting the level of successive polishing steps. The impinging electrons in SEM should be dissipated well to obtain optimal BSE images. The use of carbon coating of the polished samples does provide the solution, which can be accomplished by either the evaporation of carbon-loaded thread, or electronic carbon thickness control, or carbon rods, etc. [80].

The quality of SEM images in publications is essential for clear communication and interpretation. It is also significant to ensure reproducibility and can avoid hinderance in the way of future research directions. Blurry SEM images also cause limitation in quantitative data extraction, and cause challenges to peer reviewers in analyzing and interpreting the results and understandings. Low-resolution images in scientific papers appear due to several reasons, some of which may be unintentional, while others are the result of constraints or limitations of the research process. The common reasons for the presence of low-quality SEM images in papers may include (but not limited to) instrument limitations, sample conditions, resource constraints including time and budget, image processing and acquisition, sample size, scope of the paper, image compression, historical or legacy data, and data storage and file size. For producing focused and clear SEM images for efficient transfer of information, the stigmator tool in SEM instrument should be properly utilized.

The stigmator is one of the critical components of SEM instrument, which is responsible for maintaining the astigmatism of the electron beam and adjusting the focus of the SEM equipment. While examining the fine details of mineral structures, astigmatism can cause distorted and blurry images. The stigmator ensures the symmetry and focus of electron beam, consequently producing quality SEM images. The proper use of well-adjusted stigmator allows characteristic mineral identification, enhanced elemental analysis, quantitative analysis, and precise imaging of microstructures. It also helps in enhanced imaging of thin sections, and provide crystal clear information about crystal faces, surface roughness and other textural attributes, which are essential for understanding the formation of minerals and digging deep into the geological history of the minerals.

 doi:10.20944/preprints202310.2059.v1

Figure 11 shows wollastonite samples mounted on three stubs, as described in Table 3. Figure 12 shows the effect of layers and sputter-coating on SEM analysis by comparing wollastonite samples A, B, and C for three magnifications i.e., 5kx, 60kx, and 250kx. In the sample preparation stage, sample C was left uncoated to investigate the effect of sputter-coating, while samples A and B were coated with gold-platinum coating. It can be clearly illustrated in Figure 12 that all sample C SEM images are fuzzy, and dark with few very bright spots, and having few lines making it difficult to visualize the sample morphology. This is the charging effect, logically occurring due to the absence of conductive material coating. Another important aspect can be found by comparing the 60k and 250k SEM images of sample C with its 5k image. While charging effects are prominent in all, the SEM image with lower resolution provides better visualization features when compared to the ones at higher resolution. It suggests that whenever there are some samples where it is difficult to coat them with conductive materials, it is useful to snap SEM images at lower resolution. When comparing SEM images of samples A and B, it is observed that the morphology of the sample can be studied well with single-layered samples when compared with multiple-layered ones.

Table 3. Wollastonite samples prepared for SEM analyses.

Sample	Layer	Sputter Coating
A	Multiple	Applied
B	Single	Applied
C	Single	Not Applied

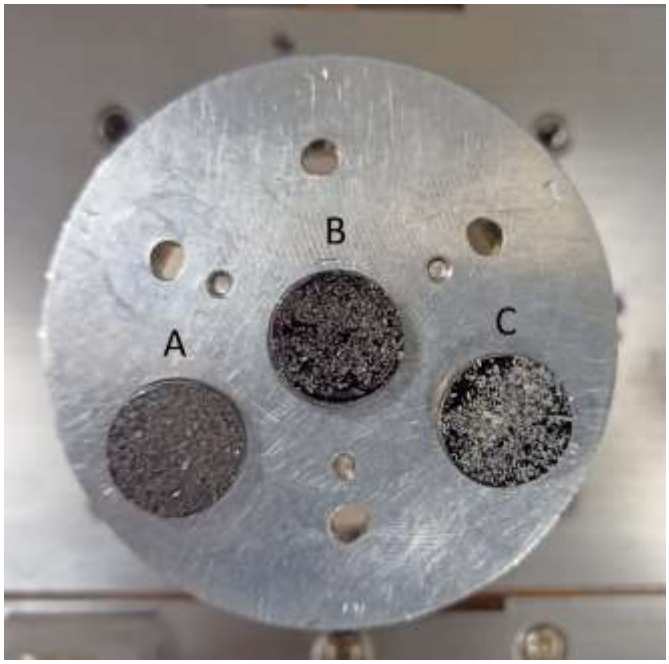

Figure 11. Wollastonite samples prepared for SEM analysis (A) multi-layer, coated (B) single layer, coated (C) single layer, uncoated.

 doi:10.20944/preprints202310.2059.v1

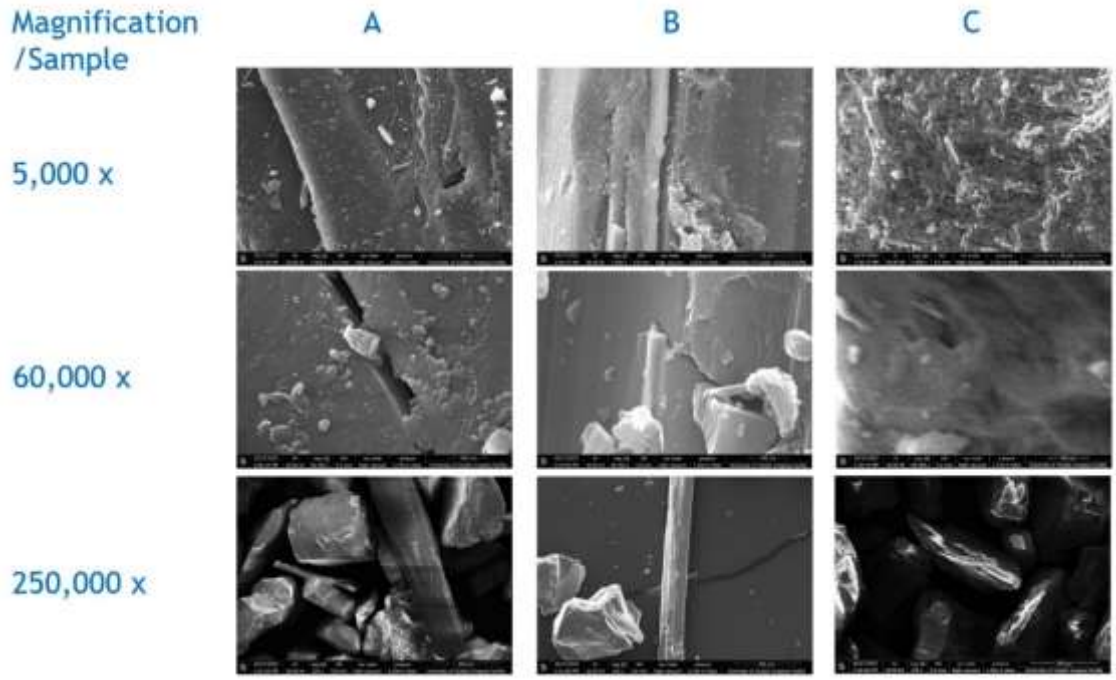

Figure 12. SEM images of wollastonite samples A, B, and C snapped at 5kx, 60kx, and 250kx magnifications.

For making sure the stigmator is well-adjusted for taking quality SEM images, the SEM instrument should be allowed to stabilize and warm up, which will comply that the electron source and other components of the instrument are in steady state before any adjustment. There are usually two stigmation modes in SEM, i.e., objective lens stigmation and condenser stigmation. The specific requirement of the imaging task will require the selection of appropriate stigmation mode. Misalignment in electron column and detectors can adversely affect the SEM image quality, that's why it is important to ensure the proper alignment of these components before starting the imaging process. Some of the latest SEMs are coming with automated alignment features. Sample preparation stage is also important for avoiding any contamination and charging effects hindering image quality. Dry, clean, and well-mounted samples provide a foundation for high-resolution SEM imaging. While focusing the electron beam on the sample, it is required to adjust the astigmatism controls to obtain a sharp image at low magnification. It is considered a good practice to select a well-defined edge or feature on the investigated sample as a reference point for stigmation control adjustments. Astigmatism is usually indicated by distortions in the SEM image, such as asymmetrical or elliptical features. In the SEM imaging process, it is important to observe such biases. The X- and Y-stigmation (representing horizontal and vertical stigmation respectively) need to be adjusted for eliminating any distortions. The focus of the electron beam should be rechecked and adjusted if necessary for proper and clear imaging. For optimal SEM imaging, several iterative adjustments might be required. **Error! Reference source not found.** compares the stigmator adjustment effect on SEM images, which vividly indicates the importance of stigmator adjustment in SEM analysis. Also, **Error! Reference source not found.** shows the effect of maintaining electron beam for a longer period of time at a single point, which damages the surface of the sample. This issue can be resolved by reducing the voltage of electron beam, but that comes at an expense of lower resolution of the SEM image. Therefore, it is recommended to find an optimum voltage-resolution combination which works well for a specific type of sample material.

 doi:10.20944/preprints202310.2059.v1

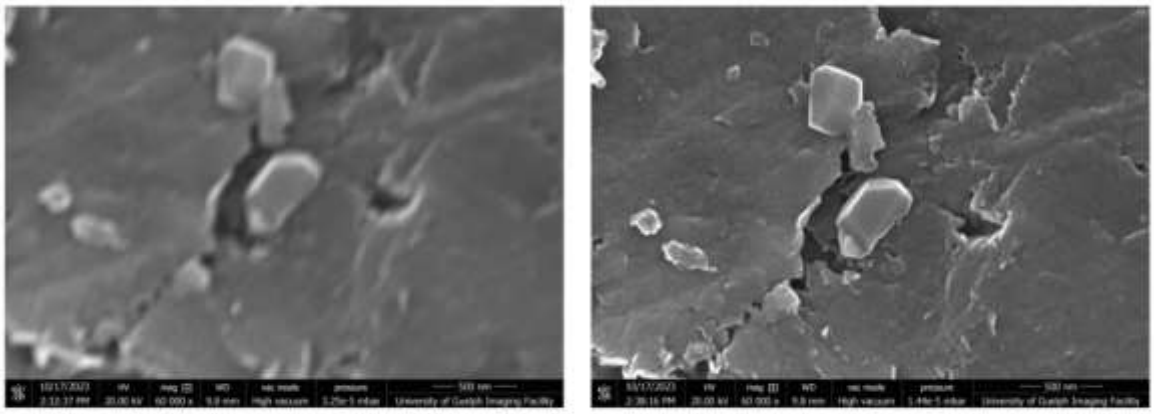

(a) (b)

Figure 13. The comparison of stigmator adjustment effect on wollastonite SEM images (a) before adjustment (b) after adjustment.

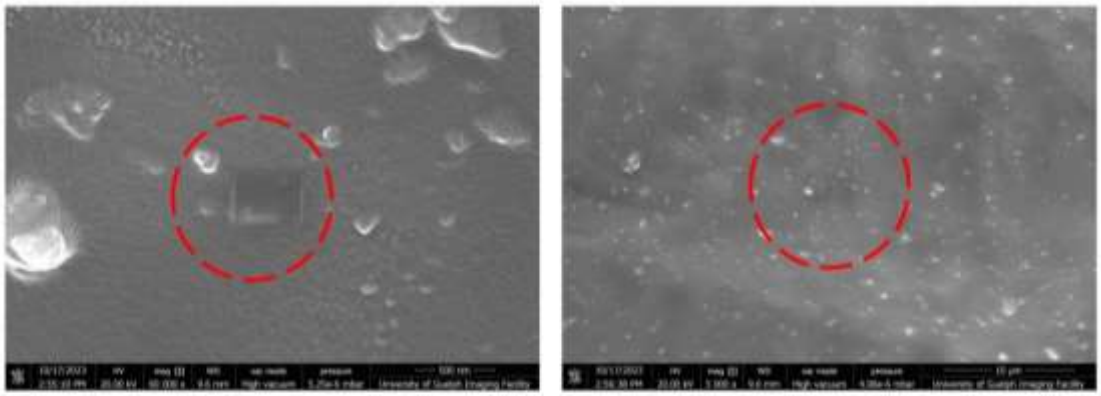

(a) (b)

Figure 14. The effect of electron beam focusing the sample for a longer period of time at (a) 60k and (b) 5k magnifications.

4. Future Research and Directions

SEM is a powerful and resourceful tool that can be employed in various fields for the analysis and characterization of minerals such as mining [179–181], oil and gas [182–184], forensic science [185–187], biomedical research [188–190], geology [191–193], material science [194–196], and environmental science [197–199]. There is an evolution witnessed in the mineral processing engineering system. Previously, there were extended levels of complexities and practical challenges in managing and optimizing a mineral processing plant, which did not make way for data-based optimization development. The empirical characterization tests were used for designing and the operator intuition played a key role in plant operation, which is subjective and varies from case to case. Now, the technology is present to make the whole process objective, which has the capability to collect, manage, and analyze the retrieved information in large amounts. These technologies, artificial intelligence (AI) and machine learning (ML) possess the revolutionizing capacity for designing, managing, operating, and analyzing mineral processing plants [200].

With the advancement of ML and deep-learning technologies, the automation of many complex tasks with human execution accuracy is becoming possible, which can replace repeating repetitive and tedious tasks, mitigate subjective human errors, lower the analysis costs, and improve the time

 doi:10.20944/preprints202310.2059.v1

efficiency of the characterization process. Deep-learning methods in microscopic imaging are now developed to automate mineral grain segmentation and recognition [201–203]. With the recent AI developments, the intelligent identification and quantification of minerals is becoming possible [204–206]. There are voids in-between geological and artificial intelligence sciences, which can be filled with the latest research advancements. This can take the SEM mineral characterization to another level, with a greater level of objective autonomy and quicker solutions for mineral analyses.

The intelligent identification of minerals can be conducted in a generally consistent process, which can be divided into five segments, i.e., mineral datasets acquisition, preprocessing mineral datasets, training the mineral identification models, validating the accuracy of mineral identification tool, and ensuring the synchronization and integration of the intelligent tool with existing SEM systems. Cai et al. recently used a multi-scale dilated convolutional attention network for rapid identification of minerals with portable Raman spectroscopy [207]. A similar approach can be used for the development of a portable intelligent SEM system. Hao et al., in the recent past, used SEM/EDS data in machine learning applications for automatically classifying the heavy minerals in river sand [208]. Likewise, models can be trained for quantifying the mineral composition of ores. In another recent work, X Zeng et al. made use of a deep convolutional neural network by combining mineral image features and hardness data, for mineral identification purposes [209]. This investigation is an intuitive way of utilizing deep learning methods for mineral characterization by integrating the mineral data sets comprising various properties. Intelligent systems based on a cascade approach for mineral identification in thin sections are already on their way for space explorations [210].

It is a matter of extending it to the SEM systems for more in-depth insights. The future research directions in SEM lead towards the possible incorporation or upgradation of such tools in SEM for enhancing the effectiveness of SEM as a material characterization tool. This would not only help in reducing the factor of human error by providing objectivity to the mineral analysis, but also by providing cost-effective solutions to those extents where human intervention has never been thought of before. It could include investigating the mineral concentration at the nano-level present in living organisms and the robotic integration of SEM tool with AI and ML for studying the mineral compositions on other planets and stars. Another idea is the integration of SEM with other material characterization tools such as XRD, and by adding the incorporation of robotics, AI, and ML, the process can be automated to a further extent. One big challenge amongst several in this research direction is the proper use of robotics for sample preparation. The system needs to be designed in a way that it first measures the conductivity and other essential properties of the objective material, then following the respective algorithms for a particular material type. The pinnacle of robotics and instrumentation can play a very important role in this development. This idea on formalization can be especially helpful for visualizing the mineral composition in locations where human intervention is usually not possible. Consider a robotic SEM-based characterization tool, trained with generative ML and AI, containing depths of mineral databases, and programmed in such a way that it is semi-controlled to choose the location of interest for scanning, and then it can go on auto-mode for scanning the raw samples and communicating real-time SEM and XRD information from depths of mines on Earth or on other terrestrial surfaces, such as the moon, mars, and other planets. In-situ and environmental SEM will facilitate the changes during the reactions. This set of information would transform the mining industry on Earth but will also revolutionize astronomical and space engineering. The developed portable SEM/ML/AI systems can help save millions of dollars for mining and space agencies. The human researchers would then be able to focus more attention on analyses, research insights, and further development of technology.

5. Conclusion

The present research review offered the synopsis of SEM fundamentals, working, sample preparation, and the imaging process. The theoretical calculations underlying basic SEM operation are discussed. This foundational set of information would be helpful for the engineers and scientists, who are inspired by the mammoth potential of SEM but have never gotten a chance to dig in-depth about the SEM operation and process. This comprehensive review briefly summarizes these multiple

 doi:10.20944/preprints202310.2059.v1

facets for efficient transfer of knowledge. In addition, the use of techniques such as energy dispersive X-ray spectroscopy EDS, automated mineralogy (AM), and mineral liberation analysis (MLA), in conjunction with SEM is discussed and research fronts are analyzed. SEM lacks statistical error, and therefore it is very important to especially look towards the uncertainties in SEM measurements. The present paper discusses the constraints in mineral phase identification by EDS. It also covers sample preparation and other analytical issues that come across while performing mineral characterization. The review then examines the possible integration of deep learning (DL), machine learning (ML), and artificial intelligence (AI) techniques into SEM to improve the robustness and objectivity of the mineral characterization process. It also discusses the idea of robotics integration with SEM for the development of portable and automated SEM units, which can collect, analyze samples, and communicate information with researchers, from locations that are difficult to explore on Earth (such as deep mines) and on other terrestrial grounds.

Author Contributions: Conceptualization, A.A. and R.M.S; writing—original draft preparation, A.A.; writing—review and editing, N.Z. and R.M.S.; supervision, R.M.S.; project administration, R.M.S.; funding acquisition, R.M.S. All authors have read and agreed to the published version of the manuscript.

Funding: This research was funded by the Natural Sciences and Engineering Research Council of Canada (NSERC), Discovery Grant 401497.

Data Availability Statement: Data is contained within the article.

Acknowledgments: The authors thank Dr. Elyse Roach and Dr. Erin Anderson from the Molecular and Cellular Imaging Facility of the University of Guelph for the training and technical assistance of the scanning electron microscope used in this study.

Conflicts of Interest: The authors declare no conflict of interest.

Nomenclature

BSE	Backscattered electron
BSEI	Backscattered electron imaging
CLI	Cathodoluminescence imaging
CSEM	Conventional scanning electron microscopy
EBIC	Electron beam induced current
EBD	Electron backscatter diffraction
EDS	Energy dispersive X-ray spectroscopy
ESEM	Environmental scanning electron microscopy
FEG SEM	Field emission gun scanning electron microscopy
LVSEM	Low vacuum scanning electron microscopy
LM	Light microscopy
MLA	Mineral liberation analysis
OM	Optical microscopy
PXMAP	Particle X-ray mapping
QEMSCAN	Quantitative evaluation of minerals by scanning electron microscopy
RPS	Rare phase search
SEI	Secondary electron imaging
SEM	Scanning electron microscopy
SPL	Sparse phase liberation analysis
SXMAP	Selected particle X-ray mapping
TEM	Transmission electron microscopy
VCI	Voltage contrast imaging
XBSE	Extended BSE liberation analysis
XRD	X-ray diffraction
XMOD	X-ray modal analysis

References

1. RRUFF - Minerals database. https://rruff.info/
2. R M Hazen, D Papineau, W Bleeker, et al. Mineral evolution. American Mineralogist 2008, 93, 1693-1720. https://doi.org/10.2138/am.2008.2955
3. C R Clarkson, M Freeman, L He, et al. Characterization of tight gas reservoir pore structure using USANS/SANS and gas adsorption analysis. Fuel 2012, 95(1), 371-385. https://doi.org/10.1016/j.fuel.2011.12.010
4. X Yu, S Li, Z Yang. Discussion on deposition-diagenesis genetic mechanism and hot issues of tight sandstone gas reservoir. Lithologic Reservoirs 2015, 27(1), 1-13. https://doi.org/10.3969/j.issn.1673-8926.2015.01.001
5. X Sui, M M Bustin, R M Bustin. Measurement of gas permeability and diffusivity of tight reservoir rocks: different approaches and their applications. Geofluids 2009, 9(3), 208-223. https://doi.org/10.1111/j.1468-8123.2009.00244.x
6. T Saif, Q Lin, A R Butcher, et al. Multi-scale multi-dimensional microstructure imaging of oil shale pyrolysis using X-ray micro-tomography, automated ultra-high resolution SEM, MAPS mineralogy, FIB-SEM. Applied Energy 2017, 202, 628-647. https://doi.org/10.1016/j.apenergy.2017.05.039
7. R D Pascoe, M R Power, B Simpson. QEMSCAN analysis as a tool for improved understanding of gravity separator performance. Minerals Engineering 2007, 20(5), 487-495. https://doi.org/10.1016/j.mineng.2006.12.012
8. J L Antoniassi, D Uliana, R Contessotto, et al. Process mineralogy of rare earths from deeply weathered alkali-carbonatite deposits in Brazil. Journal of Materials Research and Technology 2020, 9(4), 8842-8853. https://doi.org/10.1016/j.jmrt.2020.05.128
9. L Ji, J Qiu, Y Q Xia, et al. Micro-pore characteristics and methane adsorption properties of common clay minerals by electron microscope scanning. Acta Petrolie Sinica 2012, 33(2), 249-256. https://doi.org/10.7623/syxb201202009
10. B Allard, C Sotin. Determination of mineral phase percentage in granular rocks by image analysis on a microcomputer. Computer & Geosciences 1988, 14(2), 261-269. https://doi.org/10.1016/0098-3004(88)90008-8
11. K D Vernon-Parry. Scanning electron microscopy: an introduction. III-Vs Review 2000, 13(4), 40-44. https://doi.org/10.1016/S0961-1290(00)80006-X
12. M Winey, J B Meehl, E T O'toole, et al. Conventional transmission electron microscopy. Molecular Biology of the Cell 2017, 25(3). https://doi.org/10.1091/mbc.e12-12-0863
13. K C A Smith, C W Oatley. The scanning electron microscope and its fields of application. British Journal of Applied Physics 1955, 6(391). https://doi.org/10.1088/0508-3443/6/11/304
14. C Teng, Y Yuan, R Gauvin. The f-ratio quantification method applied to standard minerals with a cold field emission SEM/EDS. Talanta 2019, 204, 213-223. https://doi.org/10.1016/j.talanta.2019.05.107
15. S Ellingham, T J U Thompson, M Islam. Scanning electron microscopy-energy-dispersive x-ray (SEM/EDX): A rapid diagnostic tool to aid the identification of burnt bones and contested cremains. Journal of Forensic Sciences 2017, 63(3). https://doi.org/10.1111/1556-4029.13541
16. C Jiang, H Lu, H Zhang, et al. Recent advances on in situ SEM mechanical and electrical characterization of low-dimensional nanomaterials. Scanning 2017, 1985149, 11. https://doi.org/10.1155/2017/1985149
17. S Picazo, B Malvoisin, L Baumgartner, et al. Low temperature serpentine replacement by carbonates during seawater influx in the newfoundland margin. Minerals 2020, 10(2), 184. https://doi.org/10.3390/min10020184
18. H G Machel, R A Mason, A N Mariano, et al. Causes and emission of luminescence in calcite and dolomite. Luminescence Microscopy and Spectroscopy: Qualitative and Quantitative Applications 1991. https://doi.org/10.2110/scn.91.25.0009
19. Erol A. High-magnification SEM micrograph of siloxanes. Atomic Force Microscopy and Its Applications 2018. http://dx.doi.org/10.5772/intechopen.82076
20. H Sato, M O-Hori, K Nakayama. Surface roughness measurement by scanning electron microscope. CIRP Annals 1982, 31(1), 457-462. https://doi.org/10.1016/S0007-8506(07)63347-2
21. P Viswanathan, M G Ondeck, S Chirasatitsin, et al. 3D surface topology guides stem cell adhesion and differentiation. Biomaterials 2015, 52, 140-147. https://doi.org/10.1016/j.biomaterials.2015.01.034
22. J Wu, L Wang, L Meng. Analysis of mineral composition and microstructure of gravel aggregate based on XRD and SEM. Road Materials and Pavement Design 2017, 18, 139-148. https://doi.org/10.1080/14680629.2017.1329869
23. W Zhou, H F Greer. What can electron microscopy tell us beyond crystal structures. European Journal of Inorganic Chemistry (EurJIC) 2016, 7, 941-950. https://doi.org/10.1002/ejic.201501342
24. J A Tyburczy. Properties of rock and minerals - The electrical conductivity of rocks, minerals, and the earth. Treatise on Geophysics 2007, 2, 631-642. https://doi.org/10.1016/B978-044452748-6.00050-X

25. J D Bonilla-Jaimes, J A H Martínez, C M Luna, et al. Non-destructive in situ analysis of garnet by combining scanning electron microscopy and x-ray diffraction techniques. DYNA 2016, 83(195), 84. https://doi.org/10.15446/dyna.v83n195.46360
26. W L Sarney. Sample preparation procedure for TEM imaging of semiconductor materials. Army Research Laboratory 2004, ARL-TR-3223. https://apps.dtic.mil/sti/pdfs/AD1111666.pdf
27. C Habold, S Dunel-Erb, C Chevalier, et al. Observations of the intestinal mucosa using environmental scanning electron microscopy (ESEM); comparison with conventional scanning electron microscopy (CSEM). Micron 2003, 34(8), 373-379. https://doi.org/10.1016/S0968-4328(03)00080-5
28. G Danilatos, J Rattenberger, V Dracopoulos. Beam transfer characteristics of a commercial environmental SEM and a low vacuum SEM. Journal of Microscopy 2010, 242(2), 166-180. https://doi.org/10.1111/j.1365-2818.2010.03455.x
29. T J Van Dam. L L Sutter, K D Smith, et al. Guidelines for detection, analysis, and treatment of materials-related distress in concrete pavements. Federal Highway Administration, Research Technology and Development, Virginia 2002, 2, 246. https://rosap.ntl.bts.gov/view/dot/808
30. M B Haha, E Gallucci, A Guidoum, et al. Relation of expansion due to alkali silica reaction to the degree of reaction measured by SEM image analysis. Cement and Concrete Research 2007, 37(8), 1206-1214. https://doi.org/10.1016/j.cemconres.2007.04.016
31. S Zebbar, D Zebbar, A Kadoun. Gaseous cascade amplification in He-H2O gas mixture in an environmental scanning electron microscope. Energy Procedia 2015, 74, 205-210. https://doi.org/10.1016/j.egypro.2015.07.579
32. M Knoll, E Ruska. Das Elektronenmikroskop. Zeitschrift für Physik 1932, 78, 318-339. https://link.springer.com/article/10.1007/BF01342199
33. E Ruska. The development of the electron microscope and of electron microscopy. Bioscience Reports 1987, 7, 607-629. https://link.springer.com/article/10.1007/BF01127674
34. M von Ardenne. Das Elektronen-Rastermikroskop. Zeitschrift für Physik 1938, 109, 553-572. https://link.springer.com/article/10.1007/BF01341584
35. M von Ardenne, P Hawkes, T Mulvey. On the history of scanning electron microscopy, of the electron microprobe, and of early contributions to transmission electron microscopy. Advances in Imaging and Electron Physics 2021, 220, 25-50. https://doi.org/10.1016/bs.aiep.2021.08.002
36. J I Goldstein, D E Newbury, P Echlin, et al. Scanning electron microscopy and X-ray microanalysis. Kluwer Academic, New York 2003. ISBN: 978-1-4613-4969-3
37. P J Breton. From microns to nanometers: Early landmarks in the science of scanning electron microscope imaging. Scanning Microscopy 1999, 13(1). Link
38. G D Danilatos. Review and outline of environmental SEM at present. Journal of Microscopy 1991, 391-402. https://doi.org/10.1111/j.1365-2818.1991.tb03149.x
39. G D Danilatos. Introduction to the ESEM instrument. Microscopy Research & Technique 1993, 25, 354-361. https://doi.org/10.1002/jemt.1070250503
40. H Li, J Li, G Gu. Local field emission from individual vertical carbon nanofibers grown on tungsten filament. Carbon 2005, 43(4), 849-853. https://doi.org/10.1016/j.carbon.2004.11.021
41. C W Oatley. The tungsten filament gun in the scanning electron microscope. Journal of Physics E: Scientific Instruments 1975, 8, 1037. https://doi.org/10.1088/0022-3735/8/12/018
42. H Ahmed, A N Broers. Lanthanum hexaboride electron emitter. Journal of Applied Physics 1972, 43(5), 2185-2192. https://doi.org/10.1063/1.1661472
43. J M D Kowalczyk, M R Hadmack, E B Szarmes, et al. Emissivity of lanthanum hexaboride thermionic electron gun cathode. International Journal of Thermophysics 2014, 35, 1538-1544. https://link.springer.com/article/10.1007/s10765-014-1712-3
44. T C Isabell, V P Dravid. Resolution and sensitivity of electron backscattered diffraction in a cold field emission gun SEM. Utramicroscopy 1997, 67, 59-68. https://doi.org/10.1016/S0304-3991(97)00003-X
45. M A Harmann, S Blouin, B M Misof, et al. Quantitative backscattered electron imaging of bone using a thermionic or a field emission electron source. Calcified Tissue International 2021, 109, 190-202. https://link.springer.com/article/10.1007/s00223-021-00832-5
46. K de Haan, Z S Ballard, Y Rivenson, et al. Resolution enhancement in scanning electron microscopy using deep learning. Scientific Reports 2019, 9, 12050. https://www.nature.com/articles/s41598-019-48444-2
47. M Ramakokovhu, P A Olubambi, R K Mbaya, et al. Mineralogical and leaching characteristics of altered ilmenite beach placer sands. Minerals 2020, 10(11), 1022. https://doi.org/10.3390/min10111022
48. G T Belz, G J Auchterlonie. An investigation of the use of chromium, platinum and gold coating for scanning electron microscopy of casts of lymphoid tissues. Micron 1995, 26(2), 141-144. https://doi.org/10.1016/0968-4328(95)00055-9
49. A L Volynskii, D A Panchuk, A V Bolshakova, et al. Structure and properties of nanosized coatings deposited onto polymers. Colloid Journal 2011, 73(5), 587-604. https://doi.org/10.1134/S1061933X11050188

50. I Stokroos, D Kalicharan, J J V D Want, et al. A comparative study of thin coatings of Au/Pd, Pt and Cr produced by magnetron sputtering for FE-SEM. Journal of Microscopy 1998, 189, 79-89. https://doi.org/10.1046/j.1365-2818.1998.00282.x
51. A Agarwal, J Simonaitis, V K Goyal, et al. Secondary electron count imaging in SEM. Ultramicroscopy 2023, 245, 113662. https://doi.org/10.1016/j.ultramic.2022.113662
52. P Kejzlar, M Švec, E Macajová. The usage of backscattered electrons in scanning electron microscopy. Manufacturing Technology 2014, 14(3), 333-336. https://doi.org/10.21062/ujep/x.2014/a/1213-2489/MT/14/3/333
53. E Sánchez, M Torres Deluigi, G Castellano. Mean atomic number quantitative assessment in backscattered electron imaging. Microscopy and Microanalysis 2012, 18(6). https://doi.org/10.1017/S1431927612013566
54. E Müller, D Gerthsen. Composition quantification of electron-transparent samples by backscattered electron imaging in scanning electron microscopy. Ultramicroscopy 2017, 173, 71-75. https://doi.org/10.1016/j.ultramic.2016.12.003
55. M Čalkovský, E Müller, D Gerthsen. Quantitative analysis of backscattered-electron contrast in scanning electron microscopy. Journal of Microscopy 2022, 289(1), 32-47. https://doi.org/10.1111/jmi.13148
56. L Reimer. Scanning electron microscopy. Springer series in optical science 1985, 42. Link
57. E Palamara, P P Das, S Nicolopoulos, et al. Applying SEM-cathodoluminescence imaging and spectroscopy as an advanced research tool for the characterization of archaeological material. Microchemical Journal 2020, 158, 105230. https://doi.org/10.1016/j.microc.2020.105230
58. C M Parish, D Batchelor, C Progl, et al. Electron beam induced current in SEM. Materials Characterization Department: Sandia National Laboratories 2007. Link
59. K Suemori, Y Watanabe, N Fukuda, et al. Voltage contrast in scanning electron microscopy to distinguish conducting Ag nanowire networks from nonconducting Ag nanowire networks. ACS Omega 2020, 5(22), 12692-12697. https://doi.org/10.1021/acsomega.9b04222
60. A V Crewe, M Isaacson, D Johnson. A simple scanning electron microscope. Review of Scientific Instruments 1969, 123081517. https://doi.org/10.1063/1.1683910
61. C Li, D Wang, L Kong. Application of machine learning techniques in mineral classification for scanning electron microscopy - energy dispersive X-ray spectroscopy (SEM-EDS) images. Journal of Petroleum Sciences and Engineering 2021, 200, 108178. https://doi.org/10.1016/j.petrol.2020.108178
62. Y Wen, Y Cheng, Z Liu, et al. Application of SEM and EDS for mineral composition of shale gas reservoir. IOP Conference Series: Materials Science and Engineering 2020, 780, 042055. https://doi.org/10.1088/1757-899X/780/4/042055
63. W Nikonow, D Rammlmair. Automated mineralogy based on micro-energy-dispersive X-ray fluorescence microscopy (μ-EDXRF) applied to plutonic rock thin sections in comparison to a mineral liberation analyzer. Geoscientific Instrumentation, Methods and Data Systems 2017, 6(2), 429-437. https://doi.org/10.5194/gi-6-429-2017
64. G Pe-Piper, A Imperial, D J W Piper, et al. Mineral data (SEM, electron microprobe, Raman spectroscopy) from epithermal hydrothermal alteration of the Miocene Sigri Petrified Forest and host pyroclastic rocks, Western Lesbos, Greece. Data in Brief 2019, 24, 103987. https://doi.org/10.1016/j.dib.2019.103987
65. R M Santos, P C M Knops, K L Rijnsburger, et al. CO2 energy reactor - integrated mineral carbonation: Perspectives on lab-scale investigation and products valorization. Frontiers in Energy Research 2016, 4. https://doi.org/10.3389/fenrg.2016.00005
66. K Lammers, R Murphy, A Riendeau, et al. CO2 sequestration through mineral carbonation of iron oxyhydroxides. Environmental Science & Technology 2011, 45, 10422-10428. https://doi.org/10.1021/es202571k
67. F Haque, R M Santos, Y W Chiang. Using nondestructive techniques in mineral carbonation for understanding reaction fundamentals. Powder Technology 2019, 357, 134-138. https://doi.org/10.1016/j.powtec.2019.08.089
68. A E Zarandi, F Larachi, G Beaudoin, et al. Nesquehonite as a carbon sink in ambient mineral carbonation of ultramafic mining wastes. Chemical Engineering Journal 2017, 314, 160-168. https://doi.org/10.1016/j.cej.2017.01.003
69. H Fantucci, J S Sidhu, R M Santos. Mineral carbonation as an educational investigation of green chemical engineering design. Sustainability 2019, 11(15), 4156. https://doi.org/10.3390/su11154156
70. A Ali, Y Wai Chiang, R M Santos. X-ray diffraction techniques for mineral characterization: A review for engineers of the fundamentals, applications, and research directions. Minerals 2022, 12(2), 205. https://doi.org/10.3390/min12020205
71. H P Klug, L E Alexander. X-ray diffraction procedures: For polycrystalline and amorphous materials, 2nd edition. Wiley 1974. ISBN: 978-0-471-49369-3
72. A Ali, C E Mendes, L G T C de Melo, et al. Production of sodium bicarbonate with saline brine and CO2 co-utilization: comparing modified Solvay approaches. Crystals 2023, 13(3), 470. https://doi.org/10.3390/cryst13030470

73. G C Chi, G Xiao, Y L Chen, et al. Application of X-ray powder diffractometer in the identification and classification of phyllite. Geology and Resources 2013, 22(5), 409-414. https://doi.org/10.13686/j.cnki.dzyzy.2013.05.014
74. Z Xue-hua. Controlling factors of order degree of dolomite in carbonate rocks: A case study from lower palezoic in Tahe oilfield and Triassic in northeastern Sichuan basin. Lithologic reservoirs 2009, 21(3), 50-55. Link
75. M J Trindade, M I Dias, J Coroado, et al. Mineralogical transformations of calcareous rich clays with firing: A comparative study between calcite and dolomite rich clays from Algrave, Portugal. Applied Clay Science 2009, 42, 345-355. https://doi.org/10.1016/j.clay.2008.02.008
76. M Dri, A Sanna, M M Maroto-Valer. Mineral carbonation from metal wastes: Effect of solid to liquid ratio on the efficiency and characterization of carbonated products. Applied Energy 2014, 113, 515-523. https://doi.org/10.1016/j.apenergy.2013.07.064
77. B Reynolds, K J Reddy, M D Argyle. Field application of accelerated mineral carbonation. Minerals 2014, 4, 191-207. https://doi.org/10.3390/min4020191
78. D E Newbury, N W M Ritchie. Is scanning electron microscopy/energy dispersive x-ray spectrometry (SEM/EDS) quantitative? Scanning 2013, 35, 141-168. https://doi.org/10.1002/sca.21041
79. M Warlo, C Wanhainen, G Bark, et al. Automated quantitative mineralogy optimized for simultaneous detection of (precious/critical) rare metals and base metals in a production-focused environment. Minerals 2019, 9(7), 440. https://doi.org/10.3390/min9070440
80. B Schulz, D Sandmann, S Gilbricht. SEM-based automated mineralogy and its application in geo- and material sciences. Minerals 2020, 10(11), 1004, https://doi.org/10.3390/min10111004
81. B Schulz, G Merker, J Gutzmer. Automated SEM mineral liberation analysis (MLA) with generically labelled EDX spectra in the mineral processing of rare earth element ores. Minerals 2019, 9(9), 527, https://doi.org/10.3390/min9090527
82. D M Smythe, A Lombard, L L Coetzee. Rare earth element deportment studies utilising QEMSCAN technology. Minerals Engineering 2013, 52, 52-61, https://doi.org/10.1016/j.mineng.2013.03.010
83. G K Rollinson, J C Andersen, R J Stickland, et al. Characterisation of non-sulphide zinc deposits using QEMSCAN®. Minerals Engineering 2011, 24, 778-787, https://doi.org/10.1016/j.mineng.2011.02.004
84. C Knappett, D Pirrie, M R Power. Mineralogical analysis and provenancing of ancient ceramics using automated SEM-EDS analysis (QEMSCAN®): A pilot study on LB I pottery from Akrotiri, Thera. Journal of Archaeological Science 2011, 38, 219-232, https://doi.org/10.1016/j.jas.2010.08.022
85. M A Saghiri, K Asgar, M Lotfi, et al. Back-scattered and secondary electron images of scanning electron microscopy in dentistry: a new method of surface analysis. Acta Odontologica Scandinavica 2012, 70(6), 603-609. https://doi.org/10.3109/00016357.2011.645057
86. K O Kjellsen, A Monsøy, K Isachsen, et al. Preparation of flat-polished specimens for SEM-backscattered electron imaging and X-ray microanalysis - importance of epoxy impregnation. Cement and Concrete Research 2003, 33(4), 611-616. https://doi.org/10.1016/S0008-8846(02)01029-3
87. P Kejzlar, M Švec, E Macajová. The usage of backscattered electrons in scanning electron microscopy. Manufacturing Technology 2014, 14(3), 333-336. https://doi.org/10.21062/ujep/x.2014/a/1213-2489/MT/14/3/333
88. K F J Heinrich, H Yakowitz. Quantitative electron probe microanalysis: Fluorescence correction uncertainty. Microchimica Acta 1968, 56, 905-916. https://doi.org/10.1007/BF01221155
89. Z-S Duma, T Sihvonen, J Havukainen, et al. Optimizing energy dispersive X-ray spectroscopy (EDS) image fusion to scanning electron microscopy (SEM) images. Micron 2022, 163, 103361. https://doi.org/10.1016/j.micron.2022.103361
90. M Scimeca, S Bischetti, H K Lamsira, et al. Energy dispersive X-ray (EDX) microanalysis: A powerful tool in biomedical research and diagnosis. European Journal of Histochemistry 2018, 62(1), 2841. https://doi.org/10.4081/ejh.2018.2841
91. B G Kutchko, A G Kim. Fly ash characterization by SEM-EDS. Fuel 2006, 85, 2537-2544. https://doi.org/10.1016/j.fuel.2006.05.016
92. F Georget, W Wilson, K L Scrivener. Microstructure characterization from quantified SEM-EDS hypermaps. Cement and Concrete Research 2021, 141, 106327. https://doi.org/10.1016/j.cemconres.2020.106327
93. E J Vermeij, P D Zoon, S B C G Chang, et al. Analysis of microtraces in invasive traumas using SEM/EDS. https://doi.org/10.1016/j.forsciint.2011.07.025
94. A V Girao, G Caputo, M C Ferro. Application of scanning electron microscopy-energy dispersive X-ray spectroscopy (SEM-EDS). Comprehensive Analytical Chemistry 2017, 75, 153-168. https://doi.org/10.1016/bs.coac.2016.10.002
95. A Avula, A Galor, P Blackwelder, et al. Application of scanning electron microscopy with energy dispersive X-ray spectroscopy for analyzing ocular surface particles on schirmer strips. Cornea 2017, 36(6), 752-756. https://doi.org/10.1097/ICO.0000000000001173

96. S Han, S C Löhr, A N Abbott, et al. Earth system science applications of next-generation SEM-EDS automated mineral mapping. Frontiers in Earth Science 2022, 10. https://doi.org/10.3389/feart.2022.956912
97. D Moro, G Ulian, G Valdrè. SEM-EDS nanoanalysis of mineral composite materials: A Monte Carlo approach. Composite Structures 2021, 259, 113227. https://doi.org/10.1016/j.compstruct.2020.113227
98. A Butera, M Pascadopoli, S Gallo, et al. SEM/EDS evaluation of the mineral deposition on a polymeric composite resin of a toothpaste contacting biomimetic Zn-carbonate hydroxyapatite (microRepair®) in oral environment: A randomized clinical trial. Polymers 2021, 13(16), 2740. https://doi.org/10.3390/polym13162740
99. Y Liu, A Liu, S Liu, et al. Nano-scale mechanical properties of constituent minerals in shales investigated by combined nanoindentation statistical analyses and SEM-EDS-XRD techniques. International Journal of Rock Mechanics and Mining Sciences 2022, 159, 105187. https://doi.org/10.1016/j.ijrmms.2022.105187
100. S Sukmara, Suyanti, W A Ardi, et al. Mineral analysis and its extraction process of ilmenite rocks in titanium-rich cumulates from Pandeglang Banten Indonesia. Journal of Materials Research and Technology 2022, 17, 3384-3393. https://doi.org/10.1016/j.jmrt.2022.02.005
101. A T Weerakoon, C Cooper, I A Meyers, et al. Does dentine mineral change with anatomical location, microscopic site and patient age? Journal of Structural Biology: X 2022, 6, 10060. https://doi.org/10.1016/j.yjsbx.2022.100060
102. Y Jiang, Y Li, S Liao, et al. Mineral chemistry and 3D tomography of a Chang'E 5 high-Ti basalt: implication for the lunar thermal evolution history. Science Bulletin 2022, 67(7), 755-761. https://doi.org/10.1016/j.scib.2021.12.006
103. R Lastra. Seven practical application cases of liberation analysis. International Journal of Mineral Processing 2007, 84, 337-347. https://doi.org/10.1016/j.minpro.2006.07.017
104. K O Hoal, J G Stammer, S K Appleby, et al. Research in quantitative minerology: Examples from diverse applications. Minerals Engineering 2009, 22(4), 402-408. https://doi.org/10.1016/j.mineng.2008.11.003
105. F D Ford, C R Wercholaz, A Lee. Predicting process outcomes for Sudbury platinum-group minerals using grade-recovery modeling from mineral liberation analyzer (MLA) data. The Canadian Mineralogist 2012, 49(6), 1627. https://doi.org/10.3749/canmin.49.6.1627
106. M MacDonald, B Adair, D Bradshaw, et al. Learnings from five years of on-site MLA at Kennecott Utah Copper Corporation: (Myth busters through quantitative evidence). Proceedings of the 10th International Congress for Applied Mineralogy (ICAM) 2012, 419-426. SpringerLink
107. K F E Anderson, F Wall, G K Rollinson, et al. Quantitative mineralogical and chemical assessment of the Nkout iron ore deposit, Southern Cameroon. Ore Geology Reviews 2014, 62, 25-39. https://doi.org/10.1016/j.oregeorev.2014.02.015
108. H E Gabler, F Melcher, T Graupner, et al. Speeding up the analytical workflow for Coltan fingerprinting by an integrated mineral liberation analysis/LA-ICP-MS approach. Geostandards and Geoanalytical Research 2011. https://doi.org/10.1111/j.1751-908X.2011.00110.x
109. C Lund, P Lamberg, T Lindberg. Practical way to quantify minerals from chemical assays at Malmberget iron ore operations - an important tool for the geometallurgical program. Mineral Engineering 2013, 49, 7-16. https://doi.org/10.1016/j.mineng.2013.04.005
110. B Schulz. Polymetamorphism in garnet micaschists of the Saulape Eclogite Unit (Eastern Elps, Austria), resolved by automated SEM method and EMP-Th-U-Pb monazite dating. Journal of Metamorphic Geology 2016. https://doi.org/10.1111/jmg.12224
111. J Pszonka, B Schulz. SEM automated mineralogy applied for the quantification of mineral and textural sorting in submarine sediment gravity flows. Minerals Resources Management 2022, 38(4), 105-131. https://doi.org/10.24425/gsm.2022.144094
112. R Wessels, T Kok, H van Melick, et al. Constraining P-T conditions using a SEM automated mineralogy based workflow - an example from Cap de Creus, NE Spain. EGU General Assembly Conference 2022. https://doi.org/10.5194/egusphere-egu22-6179
113. J P Ranta, N Cook, S Gilbricht. SEM-based automated mineralogy (SEM-AM) and unsupervised machine learning studying the textural setting and elemental association of gold in the Rajapalot Au-Co area, northern Finland. Bulletin of the Geological Society of Finland 2021, 93, 129-154. https://doi.org/10.17741/bgsf/93.2.003
114. Y Gu. Automated scanning electron microscope based mineral liberation analysis. Journal of Minerals and Materials Characterization & Engineering 2003, 2(1), 33-41. https://file.scirp.org/pdf/JMMCE20030100003_64231986.pdf
115. R P King, C L Schneider. Stereological correction of linear grade distribution for mineral liberation. Powder Technology 1998, 98(1), 21-37. https://doi.org/10.1016/S0032-5910(98)00013-8
116. C Chiaruttini, L Piga, G Schena. An assessment of the efficiency of a stereological correction for recovering the volumetric grade of particles from measures on polished section. International Journal of Mineral Processing 1999, 57(4), 303-322. https://doi.org/10.1016/S0301-7516(99)00026-5

117. R G Fandrichi, C L Schneider, S L Gay. Two stereological correction methods: Allocation method and kernel transformation method. Minerals Engineering 1998, 11(8), 707-715. https://doi.org/10.1016/S0892-6875(98)00057-0
118. G M Leigh, G J Lyman, P Gottlieb. Stereological estimates of liberation from mineral section measurements: a rederivation of Barbery's formulae with extensions. Powder Technology 1996, 87, 141-152. Link
119. W R Goodall, P J Scales. An overview of the advantages and disadvantages of the determination of gold mineralogy by automated mineralogy. Minerals Engineering 2007, 20(5), 506-517. https://doi.org/10.1016/j.mineng.2007.01.010
120. D Pirrie, G K Rollinson. Unlocking the applications of automated mineral analysis. Geology Today 2011, 27(6). https://doi.org/10.1111/j.1365-2451.2011.00818.x
121. B Li, X Nie, J Cai, et al. U-Net model for multi-component digital rock modeling of shales based on CT and QEMSCAN images. Journal of Petroleum Science and Engineering 2022, 216, 110734. https://doi.org/10.1016/j.petrol.2022.110734
122. Z Liu, D Liu, Y Cai, et al. Permeability, mineral and pore characteristics of coal response to acid treatment by NMR and QEMSCAN: Insight into acid sensitivity mechanism. Journal of Petroleum Science and Engineering 2021, 198, 108205. https://doi.org/10.1016/j.petrol.2020.108205
123. S Lin, L Hou, X Luo. Shale mineralogy analysis method: Quantitative correction of minerals using QEMSCAN based on MAPS technology. Applied Sciences 2022, 12(10), 5013. https://doi.org/10.3390/app12105013
124. J Mason, E Lin, E Grono, et al. QEMSCAN® analysis of clay-rich stratigraphy associated with early agricultural contexts at Kuk Swamp, Papua New Guinea. Journal of Archaeological Science: Reports 2022, 42, 103356. https://doi.org/10.1016/j.jasrep.2022.103356
125. K Vickery, F Eckardt. A closer look at mineral aerosol emissions from the Makgadikgadi Pans, Botswana, using automated SEM-EDS (QEMSCAN®). South African Geographical Journal 2021, 103 (1). https://doi.org/10.1080/03736245.2020.1824805
126. J C Andersen, G K Rollinson, B Snook, et al. Use of QEMSCAN for the characterization of Ni-rich and Ni-poor geothite in laterite ores. Minerals Engineering 2009, 22(13), 1119-1129. https://doi.org/10.1016/j.mineng.2009.03.012
127. N A-Rodríguez, A B R-Navarro, M C D Hoces, et al. Chemical and mineralogical characterization of montevive celestine mineral. Minerals 2022, 12(10), 1261. https://doi.org/10.3390/min12101261
128. S Makvandi, P Pagé, J Tremblay, et al. Exploration for platinum-group minerals in till: A new approach to the recovery, counting, mineral identification and chemical characterization. Minerals 2021, 11(3), 264. https://doi.org/10.3390/min11030264
129. W He, K Chen, A Hayatdavoudi, et al. Effects of clay content, cement and mineral composition characteristics on sandstone rock strength and deformability behaviors. Journal of Petroleum Science and Engineering 2019, 176, 962-969. https://doi.org/10.1016/j.petrol.2019.02.016
130. Y Chen, Y Chen, Q Liu, et al. Quantifying common major and minor elements in minerals/rocks by economical desktop scanning electron microscopy/silicon drift detector energy-dispersive spectrometer (SEM/SDD-EDS). Solid Earth Sciences 2023, 8(1), 49-67. https://doi.org/10.1016/j.sesci.2022.12.002
131. Y Liu, A Liu, S Liu, et al. Nano-scale mechanical properties of constituent minerals in shales investigated by combined nanoindentation statistical analyses and SEM-EDS-XRD techniques. International Journal of Rock Mechanics and Mining Sciences 2022, 159, 105187. https://doi.org/10.1016/j.ijrmms.2022.105187
132. J McCutcheon, G Southam. Advanced biofilm staining techniques for TEM and SEM in geomicrobiology: Implications for visualizing EPS architecture, mineral nucleation, and microfossil generation. Chemical Geology 2018, 498, 115-127. https://doi.org/10.1016/j.chemgeo.2018.09.016
133. C Fowler, R J M Lynch, D Shingler, et al. A novel electron-microscopic method for measurement of mineral content in enamel lesions. Archives of Oral Biology 2018, 94, 10-15. https://doi.org/10.1016/j.archoralbio.2018.06.013
134. B Yousefi, C I Castanedo, X P V Maldague, et al. Assessing the reliability of an automated system for mineral identification using LWIR hyperspectral infrared imagery. Minerals Engineering 2020, 155, 106409. https://doi.org/10.1016/j.mineng.2020.106409
135. G Wille, D Lahondere, U Schmidt, et al. Coupling SEM-EDS and confocal Raman-in-SEM imaging: A new method for identification and 3D morphology of asbestos-like fibers in a mineral matrix. Journal of Hazardous Materials 2019, 374, 447-458. https://doi.org/10.1016/j.jhazmat.2019.04.012
136. G O Ihekweme, J N Shondo, K I Orisekeh, et al. Characterization of certain Nigerian clay minerals for water purification and other industrial applications. Heliyon 2020, 6(4), e03783. https://doi.org/10.1016/j.heliyon.2020.e03783
137. G Deshpande, J Tonannavar, J Tonannavar, et al. Detection of the mineral constituents in human renal calculi by vibrational spectroscopic analysis combined with allied techniques powder XRD, TGA, SEM, IR imaging and TXRF. Spectrochimica Acta Part A: Molecular and Biomolecular Spectroscopy 2022, 270, 120867. https://doi.org/10.1016/j.saa.2022.120867

138. E Raguin, K Rechav, R Shahar, et al. Focused ion beam-SEM 3D analysis of mineralized osteonal bone: lamellae and cement sheath structures. Acta Biomaterialia 2021, 121, 497-513. https://doi.org/10.1016/j.actbio.2020.11.002
139. S E Smith-Schmitz, M S Appold. Determination of fluorine concentrations in mineralizing fluids of the Hansonburg, New Mexico Ba-F-Pb district via SEM-EDS analysis of fluid inclusion decrepitates. Journal of Geochemical Exploration 2021, 230, 106861. https://doi.org/10.1016/j.gexplo.2021.106861
140. D J Buss, N Reznikov, M D McKee. Crossfibrillar mineral tessellation in normal and Hyp mouse bone as revealed by 3D FIB-SEM microscopy. Journal of Structural Biology 2020, 212(2), 107603. https://doi.org/10.1016/j.jsb.2020.107603
141. P Asadi, L E Beckingham. Intelligent framework for mineral segmentation and fluid-accessible surface area analysis in scanning electron microscopy. Applied Geochemistry 2022, 143, 105387. https://doi.org/10.1016/j.apgeochem.2022.105387
142. Y Wang, S Liu, L Zhang, et al. Evidence of self-sealing in wellbore cement under geologic CO2 storage conditions by micro-computed tomography (CT), scanning electron microscopy (SEM), and Raman observations. Applied Geochemistry 2021, 128, 104937. https://doi.org/10.1016/j.apgeochem.2021.104937
143. E Berrezueta, P Moita, J Pedro, et al. Laboratory experiments and modelling of the geochemical interaction of a gabbro-anorthosite with seawater and supercritical CO2: A mineral carbonation study. Geoenergy Science and Engineering 2023, 228, 212010. https://doi.org/10.1016/j.geoen.2023.212010
144. C Fu, Yi Du, W Song, et al. Application of automated mineralogy in petroleum geology and development and CO2 sequestration: A review. Marine and Petroleum Geology 2023, 151, 106206. https://doi.org/10.1016/j.marpetgeo.2023.106206
145. M Hörning, A Schertel, R Schneider, et al. Mineralized scale patterns on the cell periphery of the chrysophyte Mallomonas determined by comparative 3D cryo-FIB SEM data processing. Journal of Structural Biology 2020, 209(1), 107403. https://doi.org/10.1016/j.jsb.2019.10.005
146. G Pe-Piper, A Imperial, D J W Piper, et al. Mineral data (SEM, electron microprobe, Raman spectroscopy) from epithermal hydrothermal alteration of the Miocene Sigri Petrified Forest and host pyroclastic rocks, Western Lesbos, Greece. Data in Brief 2019, 24, 103987. https://doi.org/10.1016/j.dib.2019.103987
147. D Moro, G Ulian, G Valdré. SEM-EDS nanoanalysis of mineral composite materials: A Monte Carlo approach. Composite Structures 2021, 259, 113227. https://doi.org/10.1016/j.compstruct.2020.113227
148. A D Kamble, V A Mendhe, P D Chavan, et al. Insights of mineral catalytic effects of high ash coal on carbon conversion in fluidized bed co-gasification through FTIR, XRD, XRF, and FE-SEM. Renewable Energy 2022, 183, 729-751. https://doi.org/10.1016/j.renene.2021.11.022
149. T Farhat, Z A Disi, M Y M Ashfaq, et al. Study of diversity of mineral-forming bacteria in Sabkha mats and sediments of mangrove forest in Qatar. Biotechnology Reports 2023, e00811. https://doi.org/10.1016/j.btre.2023.e00811
150. C Fu, Q Zhan, X Zhang, et al. Self-healing properties of cement-based materials in different matrix based on microbial mineralization coupled with bimetallic hydroxide. Construction and Building Materials 2023, 400, 132686. https://doi.org/10.1016/j.conbuildmat.2023.132686
151. Y Diao, C Yang, J Huang, et al. Preparation and solidification mechanism of biomimetic mineralized cement using L-Asp as crystal modifier. Journal of Materials Research and Technology 2023, 24, 7756-7770. https://doi.org/10.1016/j.jmrt.2023.05.074
152. M S Sanchez, M M-Koerner, B D McNamee. Characterization of elongate mineral particles including talc, amphiboles, and biopyriboles observed in mineral derived powders: Comparisons of analysis of the same talcum powder samples by two laboratories. Environmental Research 2023, 230, 114791. https://doi.org/10.1016/j.envres.2022.114791
153. R Blannin, M Frenzel, L Tuşa, et al. Uncertainties in quantitative mineralogical studies using scanning electron microscope-based image analysis. Minerals Engineering 2021, 167, 106836. https://doi.org/10.1016/j.mineng.2021.106836
154. B Benvie, N M Chapman, D J Robinson, et al. A robust statistical method for mineralogical analysis in geometallurgical diagnostic leaching. Minerals Engineering 2013, 52, 178-183. https://doi.org/10.1016/j.mineng.2013.06.010
155. R Lastra, D Paktunc. An estimation of the variability in automated quantitative mineralogy measurements through inter-laboratory testing. Minerals Engineering 2016, 95, 138-145. https://doi.org/10.1016/j.mineng.2016.06.025
156. O Guseva, A K B Opitz, J L Broadhurst, et al. Characterisation and prediction of acid rock drainage potential in waste rock: Value of integrating quantitative mineralogical and textural measurements. Minerals Engineering 2021, 163, 106750. https://doi.org/10.1016/j.mineng.2020.106750
157. G M Leigh, D N Sutherland, P Gottlieb. Confidence limits for liberation measurements. Minerals Engineering 1993, 6, 155-161. https://doi.org/10.1016/0892-6875(93) 90129-B
158. C L Evans, T J Napier-Munn. Estimating error in measurements of mineral grain size distribution. Minerals Engineering 2013, 52, 198-203. https://doi.org/10.1016/j. mineng.2013.09.005

159. R A Mariano, C L Evans. Error analysis in ore particle composition distribution measurements. Minerals Engineering 2015, 82, 36-44. https://doi.org/10.1016/j. mineng.2015.06.001
160. T Leißnar, K Bachmann, J Gutzmer, et al. MLA-based partition curves for magnetic separation. Minerals Engineering 2016, 94, 94-103. https://doi.org/10.1016/j. mineng.2016.05.015
161. M Buchmann, E Schach, R Tolosana-Delgado, et al. Evaluation of magnetic separation efficiency on a cassiterite-bearing skarn ore by means of integrative SEM-based image and XRF-XRD data analysis. Minerals 2018, 8(9), 390. https://doi.org/10.3390/min8090390
162. E Schach, M Buchmann, R Tolosana-Delgado, et al. Multidimensional characterization separation processes - Part 1: Introducing kernel methods and entropy in the context of mineral processing using SEM-based image analysis. Minerals Engineering 2019, 137, 78-86. https://doi.org/10.1016/j.mineng.2019.03.026
163. J Hannula, M Kern, S Luukkanen, et al. Property-based modelling and simulation of mechanical separation processes using dynamic binning and neural networks. Minerals Engineering 2018, 126, 52-63. https://doi.org/10.1016/j.mineng.2018.06.017
164. B Efron. Bootstrap methods: Another look at the jackknife. The Annals of Statistics 1979, 7(1), 1-26. Link
165. M R Chernick. Bootstrap methods: A guide for practitioners and researchers. Applied Probability and Statistics, Wiley 1999. Link
166. F Chayes. Petrographic analysis by fragment counting: Part 1, The counting error. Economic Geology 1944, 39, 484-505. https://doi.org/10.2113/gsecongeo.39.7.484
167. F Chayes. Petrographic analysis by fragment counting: Part 2, Precision of microsampling and the combination error of sampling and counting. Economic Geology 1945, 40, 517-525. https://doi.org/10.2113/gsecongeo.40.8.517
168. L V D Plas, A C Tobi. A chart for judging the reliability of point counting results. American Journal of Science 1965, 263(1), 87-90. https://doi.org/10.2475/ajs.263.1.87
169. M Parian, P Lamberg, R Mockel, et al. Analysis of mineral grades for geometallurgy: combined element-to-mineral conversion and quantitative X-ray diffraction. Minerals Engineering 2015, 82, 25-35. https://doi.org/10.1016/J. MINENG.2015.04.023.
170. W Yuan, Q Xiao, L Li, T Xu. Thermal conductivity of epoxy adhesive enhanced by hybrid graphene oxide/AlN particles. Applied Thermal Engineering 2016, 106, 1067-1074. https://doi.org/10.1016/j.applthermaleng.2016.06.089
171. B R Jackson, A F Reid, J C Wittenberg. Rapid production of high quality polished sections for automated image analysis of minerals. Proceedings of the Australian Institute of Mining and Metallurgy 1984, 289, 93-97. Link
172. A Rahfeld, J Gutzmer. MLA-based detection of organic matter with iodized epoxy resin - an alternative to Carnauba. Journal of Minerals and Materials Characterization and Engineering 2017, 5(4). https://doi.org/10.4236/jmmce.2017.54017
173. G O'Brien, Y Gu, B J I Adair, et al. The use of optical reflected light and SEM imaging systems to provide quantitative coal characterisation. Minerals Engineering 2011, 24(12), 1299-1304. https://doi.org/10.1016/j.mineng.2011.04.024
174. C O Gomez, D W Strickler, L G Austin. An iodized mounting method for coal particles. Journal of Electron Microscopy Technique 1984, 1(3), 285-287. https://doi.org/10.1002/jemt.1060010307
175. M A Alim, M Z Abdullah, M S A Aziz, et al. Recent advances on thermally conductive adhesive in electronic packaging: A review. Polymers 2021, 13(19), 3337. https://doi.org/10.3390/polym13193337
176. G Grundmann, H Scholz, Preparation methods in mineralogy and geology: The preparation of thin sections, polished sections, acetate foil prints, preparation for Elutriation analysis and staining tests for the optical and electron microscopy. Technical University of Munich 2015. Link
177. J-R Rodríguez, M T-Lopéz, J DeFelipe, et al. Neuroanatomy from mesoscopic to nanoscopic scales: An improved method for the observation of semithin sections by high-resolution scanning electron microscopy. Frontiers in Neuroanatomy 2018, 12(14). https://doi.org/10.3389/fnana.2018.00014
178. H Ren, X Zhang, Y Li, et al. Preparation of cross-sectional membrane samples for scanning electron microscopy characterizations using a new frozen section technique. Membranes 2023, 13, 634. https://doi.org/10.3390/membranes13070634
179. Z Huang, E Yilmaz, S Cao. Analysis of strength and microstructural characteristics of mine backfills containing fly ash and desulfurized gypsum. Minerals 2021, 11(4), 409. https://doi.org/10.3390/min11040409
180. A M T Simonsen, S Solismaa, H K Hansen, et al. Evaluation of mine tailings' potential as supplementary cementitious materials based on chemical, mineralogical and physical characteristics. Waste Management 2020, 102, 710-721. https://doi.org/10.1016/j.wasman.2019.11.037
181. Q Chen, Y Tao, Y Feng, et al. Utilization of modified copper slag activated by Na2SO4 and CaO for unclassified lead/zinc mine tailings based cemented paste backfill. Journal of Environmental Management 2021, 290, 112608. https://doi.org/10.1016/j.jenvman.2021.112608

182. Z Chen, X Liu, J Yang, et al. Deep learning-based method for SEM image segmentation in mineral characterization, an example from Duvernay Shale samples in Western Canada Sedimentary Basin. Computers & Geosciences 2020, 138, 104450. https://doi.org/10.1016/j.cageo.2020.104450
183. X Liu, S-W Meng, Z-Z Liang, et al. Microscale crack propagation in shale samples using focused ion beam scanning electron microscopy and three-dimensional numerical modeling. Petroleum Science 2023, 20(3), 1488-1512. https://doi.org/10.1016/j.petsci.2022.10.004
184. N Golsanami, M N Jayasuriya, W Yan, et al. Characterizing clay textures and their impact on the reservoir using deep learning and Lattice-Boltzmann simulation applied to SEM images. Energy 2022, 240, 122599. https://doi.org/10.1016/j.energy.2021.122599
185. D Pirrie, A J Pidduck, D E Crean, et al. Identification and analysis of man-made geological product particles to aid forensic investigation of provenance in the built environment. Forensic Science International 2019, 305, 109974. https://doi.org/10.1016/j.forsciint.2019.109974
186. H S Kikkawa, K Naganuma, K Kumisaka, et al. Semi-automated scanning electron microscopy energy dispersive X-ray spectrometry forensic analysis of soil samples. Forensic Science International 2019, 305, 109947. https://doi.org/10.1016/j.forsciint.2019.109947
187. Y C Lim, A Marolf, N Estoppey, et al. A probabilistic approach towards source level inquiries for forensic soil examination based on mineral counts. Forensic Science International 2021, 328, 111035. https://doi.org/10.1016/j.forsciint.2021.111035
188. J Babilotte, V Guduric, D L Nihouannen, et al. 3D printed polymer-mineral composite biomaterials for bone tissue engineering: Fabrication and characterization. Journal of Biomedical Materials Research 2019, 107(8), 2579-2595. https://doi.org/10.1002/jbm.b.34348
189. N B Pradeep, M M R Hegde, G C M Patel, et al. Synthesis and characterization of mechanically alloyed nanostructured ternary titanium based alloy for bio-medical applications. Journal of Materials Research and Technology 2022, 16, 88-101. https://doi.org/10.1016/j.jmrt.2021.11.101
190. S Dessai, M Ayyanar, S Amalraj, et al. Bioflavonoid mediated synthesis of TiO2 nanoparticles: Characterization and their biomedical applications. Materials Letters 2022, 311, 131639. https://doi.org/10.1016/j.matlet.2021.131639
191. W Lou, D Zhang, R C Bayless. Review of mineral recognition and its future. Applied Geochemistry 2020, 122, 104727. https://doi.org/10.1016/j.apgeochem.2020.104727
192. J Maitre, K Bouchard, L P Bédard. Mineral grains recognition using computer vision and machine learning. Computers & Geosciences 2019, 130, 84-93. https://doi.org/10.1016/j.cageo.2019.05.009
193. Y Li, J Chen, D Elsworth, et al. Nanoscale mechanical property variations concerning mineral composition and contact of marine shale. Geoscience Frontiers 2022, 13(4), 101405. https://doi.org/10.1016/j.gsf.2022.101405
194. C Zhang, Y Luo, J Tan, et al. High-throughput production of cheap mineral-based two-dimensional electrocatalysts for high-current-density hydrogen evolution. Nature Communications 2020, 11, 3724. Link
195. Z Li, S Liu, W Ren, et al. Multiscale laboratory study and numerical analysis of water-weakening effect on shale. Advances in Materials Science and Engineering 2020, 5263431. https://doi.org/10.1155/2020/5263431
196. J Xie, H Ping, T Tan, et al. Bioprocess-inspired fabrication of materials with new structures and functions. Progress in Materials Science 2019, 105, 100571. https://doi.org/10.1016/j.pmatsci.2019.05.004
197. A Lu, Y Li, H Ding, et al. Photoelectric conversion on Earth's surface via widespread Fe- and Mn-mineral coatings. Earth Atmospheric and Planetary Sciences 2019, 116(20), 9741-9746. https://doi.org/10.1073/pnas.1902473116
198. A Maged, S Kharbish, I S Ismael, et al. Characterization of activated bentonite clay mineral and the mechanisms underlying its sorption for ciprofloxacin from aqueous solution. Environmental Science and Pollution Research 2020, 27, 32980-32997. Link
199. U Rao, A Iddya, B Jung, et al. Mineral scale prevention on electrically conducting membrane distillation membranes using induced electrophoretic mixing. Environmental Science & Technology 2020, 54, 6, 3678-3690. https://doi.org/10.1021/acs.est.9b07806
200. M Jooshaki, A Nad, S Michaux. A systematic review on the applications of machine learning in exploiting mineralogical data in mining and mineral industry. Minerals 2021, 11, 816. https://doi.org/10.3390/min11080816
201. G Latif, K Bouchard, J Maitre, et al. Deep-learning-based automatic mineral grain segmentation and recognition. Minerals 2022, 12, 455. https://doi.org/10.3390/min12040455
202. M Ge, F Su, Z Zhao, et al. Deep learning analysis on microscopic imaging in materials science. Materials Today Nano 2020, 11, 100087. https://doi.org/10.1016/j.mtnano.2020.100087
203. F L Rosa, R S-Reolid, J L G-Sirvent, et al. A review on machine and deep learning for semiconductor defect classification in scanning electron microscope images. Applied Science 2021, 11(20), 9508. https://doi.org/10.3390/app11209508

204. T Long, Z Zhou, G Hancke, et al. A review of artificial intelligence technologies in mineral identification: Classification and visualization. Journal of Sensor and Actuator Networks 2022, 11, 50. https://doi.org/10.3390/jsan11030050
205. A G-Flores, S Ilyas, G W Heyes, et al. A critical review of artificial intelligence in mineral concentration. Minerals Engineering 2022, 189, 107884. https://doi.org/10.1016/j.mineng.2022.107884
206. B H Bac, H Nguyen, N T Thao, et al. Performance evaluation of nanotubular halloysites from weathered pegmatites in removing heavy metals from water through novel artificial intelligence-based models and human-based optimization algorithm. Chemosphere 2021, 282, 131012. https://doi.org/10.1016/j.chemosphere.2021.131012
207. Y Cai, D Xu, H Shi. Rapid identification of ore minerals using multi-scale dilated convolutional attention network associated with portable Raman spectroscopy. Spectrochimica Acta Part A: Molecular and Biomolecular Spectroscopy 2022, 267, 120607. https://doi.org/10.1016/j.saa.2021.120607
208. H Hao, R Guo, Q Gu, et al. Machine learning application to automatically classify heavy minerals in river sand by using SEM/EDS data. Minerals Engineering 2019, 143, 105899. https://doi.org/10.1016/j.mineng.2019.105899
209. X Zeng, Y Xiao, X Ji, et al. Mineral identification based on deep learning that combines image and Mohs hardness. Minerals 2021, 11(5), 506. https://doi.org/10.3390/min11050506
210. H Izadi, J Sadri, M Bayati. An intelligent system for mineral identification in thin sections based on a cascade approach. Computers and Geosciences 2017, 99, 37-49. https://doi.org/10.1016/j.cageo.2016.10.010